

Ionized Carbon in Galaxies: The [C II] 158 μm Line as a Total Molecular Gas Mass Tracer Revisited*

YINGHE ZHAO,^{1,2} JIAMIN LIU,^{1,3} ZHI-YU ZHANG,^{4,5} AND THOMAS G. BISBAS⁶

¹*Yunnan Observatories, Chinese Academy of Sciences, Kunming 652016, China*

²*Key Laboratory of Radio Astronomy and Technology (Chinese Academy of Sciences), A20 Datun Road, Chaoyang District, Beijing, 100101, P. R. China*

³*University of Chinese Academy of Sciences, Beijing 100049, China*

⁴*School of Astronomy and Space Science, Nanjing University, Nanjing 210093, China*

⁵*Key Laboratory of Modern Astronomy and Astrophysics, Nanjing University, Ministry of Education, Nanjing 210093, China*

⁶*Research Center for Astronomical Computing, Zhejiang Lab, Hangzhou 311100, China*

ABSTRACT

In this paper we present a statistical study of the [C II] 158 μm line and the CO(1–0) emission for a sample of ~ 200 local and high- z (32 sources with $z > 1$) galaxies with much different physical conditions. We explore the correlation between the luminosities of [C II] and CO(1–0) lines, and obtain a strong linear relationship, confirming that [C II] is able to trace total molecular gas mass, with a small difference between (U)LIRGs and less-luminous galaxies. The tight and linear relation between [C II] and CO(1–0) is likely determined by the average value of the observed visual extinction A_V and the range of G_0/n in galaxies. Further investigations into the dependence of $L_{[\text{C II}]} / L_{\text{CO}(1-0)}$ on different physical properties show that $L_{[\text{C II}]} / L_{\text{CO}(1-0)}$ (1) anti-correlates with Σ_{IR} , and the correlation becomes steeper when $\Sigma_{\text{IR}} \gtrsim 10^{11} L_{\odot} \text{kpc}^{-2}$; (2) correlates positively with the distance from the main sequence $\Delta(\text{MS})$ when $\Delta(\text{MS}) \lesssim 0$; and (3) tends to show a systematically smaller value in systems where the [C II] emission is dominated by ionized gas. Our results imply that caution needs to be taken when applying a constant [C II]-to- M_{mol} conversion factor to estimate the molecular gas content in extreme cases, such as galaxies having low-level star formation activity or high SFR surface density.

Keywords: galaxies: evolution — galaxies: star formation — galaxies: ISM — galaxies: starburst — infrared: ISM

1. INTRODUCTION

Star formation (SF) converts gas into stars, and thus is one of the most fundamental drivers of galaxy evolution. To better understand the relation between SF and molecular gas, it is crucial to know the molecular gas content, which has usually been traced by the low- J transitions of carbon monoxide (CO; e.g., Solomon & Vanden Bout 2005; Bolatto et al. 2013), in external galaxies. However, it becomes challenging to detect the low- J CO transitions in higher redshift galaxies due to (1) the limited sensitivities of currently available ground facilities; (2) the combination of low excitation temperature of CO(1–0) and increasing cos-

mic microwave background (e.g., Zhang et al. 2016), reducing the observable brightness temperature contrast of the line (e.g., Riechers et al. 2020); and (3) the decreasing metal content, causing weaker CO emission (and it would no longer trace H₂ gas under extremely metal-poor conditions; e.g., Shi et al. 2015). Therefore, it is important to have some alternative H₂ tracers, as more and more galaxies have been identified at high redshifts, with some quasars and other emission-line galaxies discovered at extremely high redshifts of $z > 7$ (e.g., Finkelstein et al. 2013; Watson et al. 2015; Venemans et al. 2017; Bañados et al. 2018; Bouwens et al. 2022).

Recently, the [C I] emission ([C I] $^3\text{P}_1 \rightarrow ^3\text{P}_0$ at 492.161 GHz, hereafter [C I](1–0); and $^3\text{P}_2 \rightarrow ^3\text{P}_1$ at 809.344 GHz, hereafter [C I](2–1)) has been proposed and observationally confirmed its potential as a total molecular gas mass (M_{mol}) tracer

Corresponding author: Yinghe Zhao
zhaoyinghe@ynao.ac.cn

* Released on XX, XX, XXXX

(e.g. Papadopoulos & Greve 2004; Walter et al. 2011; Lo et al. 2014; Offner et al. 2014; Jiao et al. 2017, 2019; Valentino et al. 2018, 2020a; Dunne et al. 2022). However, the [C I] lines are generally faint and thus they are more difficult to detect at high redshifts. For $z \gtrsim 4$, there are only about twenty lensed sources detected in [C I](1–0) and/or [C I](2–1), and most of which are marginally detected with a signal-to-noise ratio (S/N) of 3 – 5 (and specially true for the [C I](1–0) line; Urquhart et al. 2022; Gururajan et al. 2023 and references therein; Hagimoto et al. 2023). Furthermore, low [C I](1–0)-to-CO ratio has also been found in local luminous infrared galaxies (LIRGs; $L_{\text{IR}}[8-1000\mu\text{m}] > 10^{11} L_{\odot}$; Sanders & Mirabel 1996) such as NGC 6052 and NGC 7679 (Michiyama et al. 2020, 2021), and in some strongly lensed sources at high- z (Harrington et al. 2021), which might be due to the subthermal excitation (Papadopoulos et al. 2022) and/or to the presence of an α -enhanced ISM (Bisbas et al. 2024), and thus challenge its capability of tracing total molecular gas mass.

Alternatively, the [C II] $^2\text{P}_{3/2} \rightarrow ^2\text{P}_{1/2}$ fine-structure transition at $158\ \mu\text{m}$ (1900.5 GHz; hereafter [C II]) might be a promising tool to probe the gas content in the distant Universe (e.g. Carilli & Walter 2013; Zanella et al. 2018, hereafter Z18; Dessauges-Zavadsky et al. 2020; Madden et al. 2020; Heintz et al. 2021; Sommovigo et al. 2021; Vizgan et al. 2022), due to the fact that (1) It can arise from all the three phases of gas, being able to be excited via collisions with electrons, atomic and molecular hydrogen with relatively low critical densities (e.g., Goldsmith et al. 2012); (2) The [C II] emission is a dominant coolant of the neutral gas and in general the most luminous single far-infrared (FIR) line in star-forming galaxies, accounting for 0.1% – 1% of the total FIR luminosity (e.g., Stacey et al. 1991; Malhotra et al. 2001; Díaz-Santos et al. 2017), and thus making it easy to detect in high- z sources (e.g., Bakx et al. 2020, $z = 8.31$; Glazer et al. 2023, a low-mass galaxy at $z \sim 6.3$; Hygate et al. 2023, $z = 7.31$; Schouws et al. 2023, $z \sim 7$); and/or (3) The dust continuum, another alternative to CO and a widely used tracer of M_{mol} (e.g. Santini et al. 2010; Magdis et al. 2012; Scoville et al. 2014, 2016), is fainter at higher redshifts due to cosmic dimming, lower metallicities and radiative transfer with the CMB (da Cunha et al. 2013; Zhang et al. 2016). Indeed, sources with strong FIR line emission but weak dust continuum have been found at $z \sim 2.5$ (Ferkinhoff et al. 2015) and $z \sim 5$ (Decarli et al. 2014; Capak et al. 2015).

However, it is necessary to validate the reliability of the [C II] emission as a total *molecular* gas mass tracer

due to the following reasons. Firstly, the gas masses in Z18 are obtained with different methods (i.e., conversion from CO luminosity and Kennicutt-Schmidt (KS hereafter) relation in Sargent et al. 2014), which might introduce bias to some extent. Secondly, as already noted in Z18, their sample galaxies with available M_{mol} estimates (see the top panel in their Figure 8) are dominated by main-sequence systems, and include few local extreme SF galaxies (e.g., ULIRGs) and low-SFE objects (e.g., early-type galaxies, hereafter ETGs; please see the proposed application of [C II] in distant quiescent sources in D’Eugenio et al. 2023). The [C II] flux in these two types of sources might be dominated by different gas phases (e.g., neutral gas from photodissociation regions (PDRs) vs diffuse ionized gas; Lu et al. 2015; Croxall et al. 2017) because of their much different physical environments (for example, [C II] might be saturate at high SFR surface density; e.g., Muñoz & Oh 2016; Ferrara et al. 2019; Bisbas et al. 2022). Thirdly, the relative carbon-to-oxygen abundance ratio, an important ISM parameter affecting the [C II]-to-CO(1–0) flux ratio as revealed by the latest astrochemical modelling (Bisbas et al. 2024), may be varied in different redshifts and/or different types of galaxies (such as discussed in Zhang et al. 2018a). Therefore, a more consistent way, using a heterogeneous data set covering a larger parameter space, is needed to check the capability of the [C II] emission as a tracer of M_{mol} .

In this paper we present our comparison between the CO(1–0) and [C II] emission for a large sample (~ 200 members) of local and high- z galaxies, including gas-rich ETGs, main-sequence sources, and (U)LIRGs. Combining with other FIR lines such [N II] and [O III] $88\ \mu\text{m}$, it also allows us to investigate the properties of [C II] emission under different physical conditions and thus to further explore its reliability of tracing the total molecular gas in galaxies. The remainder of this paper is organized as follows: we give a brief introduction of the sample, observations and data reduction in Section 2, present the results and discussion in Section 3, and briefly summarize the main conclusions in the last section. Throughout the paper, we adopt a Hubble constant of $H_0 = 70\ \text{km s}^{-1}\ \text{Mpc}^{-1}$, $\Omega_{\text{M}} = 0.28$, and $\Omega_{\Lambda} = 0.72$, which are based on the five-year WMAP results (Hinshaw et al. 2009), and are the same as those used by the Great Observatories All-Sky LIRGs Survey (GOALS; Armus et al. 2009).

2. SAMPLE AND DATA

2.1. Main Sample

Our approach cross-calibrates [C II] as a gas mass tracer through a comparison with CO(1–0) emission,

utilizing the feature that the CO(1–0) line can trace the total molecular gas in galaxies, and thus it relies on the gas mass obtained with CO(1–0)-to-H₂ conversion factor α_{CO} . As discussed in Bisbas et al. (2021, and references therein), α_{CO} is more sensitive to metallicity (Z) rather than the FUV intensity or the cosmic ray ionization rate and is likely to have an upturn with decreasing metallicity below $1/3 \sim 1/2 Z_{\odot}$ (Bolatto et al. 2013). Furthermore, the metallicity-dependent α_{CO} obtained by different works show a much larger spread when $Z \lesssim 0.5Z_{\odot}$ (e.g., see Figure 10b in Madden et al. 2020). Therefore, we select sources (1) having both CO and [C II] data available in the literature, and (2) likely being metal-rich ($Z \gtrsim 0.5 Z_{\odot}$) according to the stellar mass-metallicity (gas phase) relations for local (Tremonti et al. 2004; i.e., $Z \sim Z_{\odot}$ at stellar mass M_{\star} of $\sim 10^{9.2} M_{\odot}$) and high- z (Sanders et al. 2023, and references therein; i.e., $Z \gtrsim 0.5Z_{\odot}$ for $M_{\star} \sim 10^{9-10} M_{\odot}$ at $z = 0.8 - 3.3$) galaxies. In order to explore the [C II]’s capability of tracing the total molecular gas mass under different physical conditions, we include different types of galaxies at various redshifts. We briefly describe the properties of different subsample in the following.

(1) *Local ETGs* (Lapham et al. 2017). This sample includes 20 massive early-type sources with stellar mass of $M_{\star} \sim 10^{9.7} - 10^{11} M_{\odot}$, which are estimated using the K -band absolute magnitudes given in Cappellari et al. (2011) and a typical mass-to-light ratio of $M_{\star}/L_K = 0.6$ in solar units (Bell et al. 2003) for a Kroupa initial mass function (IMF; Kroupa 2002). The star formation rates (SFRs) are in the range of ~ 0.01 –several $M_{\odot} \text{ yr}^{-1}$ (Davis et al. 2014). They were observed with the *Herschel*/PACS, and a part were also observed with the *Herschel*/SPIRE. The [C II] data are adopted from Lapham et al. (2017), and CO data are adopted from Young et al. (2009), Crocker et al. (2011) and Alatalo et al. (2013). We also collect metallicity measurements (Maragkoudakis et al. 2018; De Vis et al. 2019; Griffith et al. 2019) for six sources. In addition, we derive the metallicities, $12 + \log(\text{O}/\text{H}) = 8.68$ and 8.83 respectively for IC1024 and UGC06176, using the emission line data from Cattorini et al. (2023) and the O3N2 estimator from Pettini & Pagel (2004, hereafter PP04).

(2) *Main sequence (MS) galaxies at $z \sim 0.01 - 0.02$* (Accurso et al. 2017b). This sample is contains 23 objects with low-to-intermediate stellar mass ($10^9 - 10^{10} M_{\odot}$), and with SFRs in the range of $\sim 0.1 - 5 M_{\odot} \text{ yr}^{-1}$. The gas-phase metallicities are larger than $\sim 0.5 Z_{\odot}$ (Accurso et al. 2017b). They have *Herschel*/PACS [C II] and IRAM CO(1–0) observations.

(3) *H-ATLAS survey, with galaxies at $z = 0.02 - 0.2$* (Ibar et al. 2015). This sample of galaxies is a mixture of normal star-forming sources and LIRGs, with $L_{\text{IR}} \sim 10^{10} - 10^{12} L_{\odot}$ and $M_{\star} \sim 10^{10} - 10^{11} M_{\odot}$, and is selected from the *Herschel*-Astrophysical Terahertz Large Area Survey (H-ATLAS; Eales et al. 2010). They were observed with *Herschel*/PACS for the [C II] emission (Ibar et al. 2015) and with ALMA for the CO(1–0) line (Villanueva et al. 2017; also see Hughes et al. 2017). In total 24 objects have both [C II] and CO(1–0) detections, and 9 out of which have their metallicity available (Ibar et al. 2015).

(4) *GOALS LIRGs* (Díaz-Santos et al. 2017). This sample of galaxies includes 75 sources with both [C II] and CO(1–0) data available, including 65 LIRGs and 10 ULIRGs with $L_{\text{IR}} > 10^{12} L_{\odot}$ and $M_{\star} \sim 10^{10} - 10^{12} M_{\odot}$ (Howell et al. 2010; U et al. 2012), observed with the *Herschel* PACS and SPIRE. The CO(1–0) data for 71 out of these sources are collected by (Jiao et al. 2017, and references therein), and for the rest 4 sources are adopted from Mirabel et al. (1990), Casoli et al. (1996), Yamashita et al. (2017) and Montoya Arroyave et al. (2023). For 13 sources the metallicities are adopted from Pérez-Díaz et al. (2024), who derived the chemical abundances using fine-structure lines in the mid- to far-infrared range (Fernández-Ontiveros et al. 2021). To match the abundances measured with the PP04 calibration, we add ~ 0.1 dex, which is obtained by comparing the metallicities of about 30 sources measured with both methods (Y. Zhao et al. 2024, in preparation), to the IR-based values. For additional 35 objects, we calculate their metallicities using the integrated line fluxes presented in Moustakas & Kennicutt (2006) and the PP04 calibration.

(5) *Local ULIRGs* (Farrah et al. 2013; Herrera-Camus et al. 2018). This sample of galaxies, which represent the most extreme starburst/AGN systems in the local Universe, include 21 members having both [C II] and CO(1–0) observations. There is no systematic determination of stellar mass and metallicity for this sample objects since it is complicated by contributions from AGN and by the range of obscurations. Nevertheless, Hou et al. (2011) find that ULIRGs have stellar masses of $10^{10} - 10^{12} M_{\odot}$, and Rupke et al. (2008) and Kilerci Eser et al. (2014) find that local ULIRGs have a nearly Solar metallicity ($12 + \log(\text{O}/\text{H}) = 8.69$; Asplund et al. 2009). The CO(1–0) data are collected from Mirabel et al. (1990), Alloin et al. (1992), Solomon et al. (1997), Baan et al. (2008), Xia et al. (2012) and Montoya Arroyave et al. (2023), and the metallicities for 3 sources are taken from Rupke et al. (2008) and Kilerci Eser et al. (2014), which have been

converted to the PP04 calibration using the correlation provided in Kewley & Ellison (2008).

(6) *Lyman-break analogs (LBAs) at $z \sim 0.2$* (Contursi et al. 2017). This sample of LBAs, which are UV luminous ($L_{UV} > 2 \times 10^{10} L_{\odot}$) and ultra-compact (UV surface brightness $I_{1530\text{\AA}} > 10^9 L_{\odot} \text{ kpc}^{-2}$) galaxies (Heckman et al. 2005) at redshift $z \sim 0.1 - 0.3$, includes 6 members with their infrared luminosities similar to local LIRGs and SFRs in the range of $15 - 110 M_{\odot} \text{ yr}^{-1}$. They have stellar masses of $M_{\star} \sim 10^{9.8} - 10^{10.9} M_{\odot}$, and metallicities of $\sim 0.5 - 1 Z_{\odot}$ (e.g., see Overzier et al. 2009). These sources were observed with the *Herchel*/PACS for [C II] and with IRAM for CO(1-0).

(7) *Intermediate to high redshift galaxies ($z \sim 0.3 - 6$)*. This sample of galaxies include 5 (U)LIRGs at redshift $z \sim 0.3$ (Magdis et al. 2014), 12 submillimetre galaxies (SMGs) and QSOs with $z = 2 - 6$ (Thomson et al. 2012; Carilli & Walter 2013; Magdis et al. 2014; Rawle et al. 2014; Capak et al. 2015; Malhotra et al. 2017; Zhang et al. 2018b; Leung et al. 2019; Riechers et al. 2020), and 20 sources ($z \sim 1 - 6$) with the CO observed in the 2-1 transition (Stacey et al. 2010; Carilli & Walter 2013; Ferkinhoff et al. 2014; Huynh et al. 2014; Pavesi et al. 2018, 2019; Cunningham et al. 2020; Riechers et al. 2020). These sources are generally massive systems with $M_{\star} \gtrsim 10^{10} M_{\odot}$ (e.g., Hainline et al. 2011; Michałowski et al. 2012), and among the 20 objects with $z > 4$, eight have $z > 5$. As in Gullberg et al. (2015), we have adopted a CO(2-1)-to-CO(1-0) flux (W m^{-2}) ratio of 7.2 (i.e., a brightness temperature ratio r_{21} of 0.9) to convert the CO(2-1) flux to the CO(1-0) flux. While the adopted r_{21} is a reasonable value based on several observational results (Bothwell et al. 2013; Aravena et al. 2014; Spilker et al. 2014; Reuter et al. 2023), and consistent with that ($r_{21} = 0.88 \pm 0.07$) from turbulence model in Harrington et al. (2021), it might introduce an additional scatter of about 0.14 dex in the CO luminosity given the observed range of $r_{21} \sim 0.6 - 1.2$. Three sources have their oxygen abundances estimated in the literature (HLSW-01: Rigopoulou et al. 2018; SDP.81: Rybak et al. 2023; SPT0418-47: Pérez-Díaz et al. 2024) and another three (SWIRE5: Pereira-Santaella et al. 2019; HDF850.1: Herard-Demanche et al. 2023; GN10: Sun et al. 2024) have optical lines flux measurements, for which the metallicities are derived and converted to the PP04 calibration.

In total there are 206 galaxies having both [C II] and CO data, and the typical uncertainties of CO and [C II] line fluxes are about 20% and 13% respectively. Auxiliary data for a part of the sample galax-

ies (specially for GOALS LIRGs; see Díaz-Santos et al. 2017) are also available, such as the [O III] $88 \mu\text{m}$, [N II] $205 \mu\text{m}$ (Zhao et al. 2016b; Lu et al. 2017), and FIR size (Lutz et al. 2016). For the CO line luminosity measured in L_{\odot} (hereafter $L_{\text{CO}(1-0)}$), it is related to that expressed in units of $\text{K km s}^{-1} \text{ pc}^2$ (L'_{CO} ; Solomon & Vanden Bout 2005) as,

$$L'_{\text{CO}} = 2.04 \times 10^4 L_{\text{CO}}. \quad (1)$$

2.2. Comparison Samples

To have a more comprehensive understanding of the relation between [C II] and CO emissions, we also include the following samples of Galactic and extragalactic regions/nuclei and metal-poor, dwarf galaxies for comparison.

(1) *Galactic/Extragalactic regions* (Stacey et al. 1991; Fadda et al. 2021). The Galactic data include 9 giant molecular clouds (GMC) and 20 H II regions, and the extragalactic nuclei contain 25 points, consisting of 14 main-sequence (i.e., dust temperature $T_{\text{dust}} < 40 \text{ K}$) and 11 star-forming ($T_{\text{dust}} > 40 \text{ K}$) regions (Stacey et al. 1991). We further add the 12 main-sequence regions in NGC 7469 presented in Fadda et al. (2021).

(2) *Dwarf galaxies* (Madden et al. 2020; Minchin et al. 2022). This sample of galaxies include 15 members, thirteen out of which have $Z \sim 0.15 - 0.5 Z_{\odot}$ and two have $Z \sim 0.7 Z_{\odot}$. For 12 out of these sources, the [C II] and CO(1-0) data are provided in Z18. For the remaining 3 galaxies from the Virgo cluster, the CO data are adopted from Grossi et al. (2016), and the [C II] data are given in Minchin et al. (2022).

3. RESULTS AND DISCUSSION

3.1. Correlation between [C II] and CO(1-0) Line Luminosities

In Figure 1 we plot the correlation between $L_{\text{CO}(1-0)}$ and $L_{[\text{C II}]}$, with red and green symbols respectively representing (U)LIRGs (i.e., $L_{\text{IR}} > 10^{11} L_{\odot}$) and normal galaxies (i.e., $L_{\text{IR}} < 10^{11} L_{\odot}$). As shown in the figure, the CO(1-0) emission is well correlated with the [C II] line. The corresponding Spearman's rank correlation coefficients, ρ , which assesses how well an arbitrary monotonic function could describe the relationship between two variables, of the trends are 0.85, 0.91, and 0.94 for (U)LIRGs, normal galaxies and the whole sample, respectively, with the probabilities (p) for the null hypothesis of no correlation between $L_{\text{CO}(1-0)}$ and $L_{[\text{C II}]}$ are ≈ 0 .

To investigate the quantitative relationship between $L_{\text{CO}(1-0)}$ and $L_{[\text{C II}]}$, we fitted each subsample using an unweighted least-squares bisector with a linear form, as

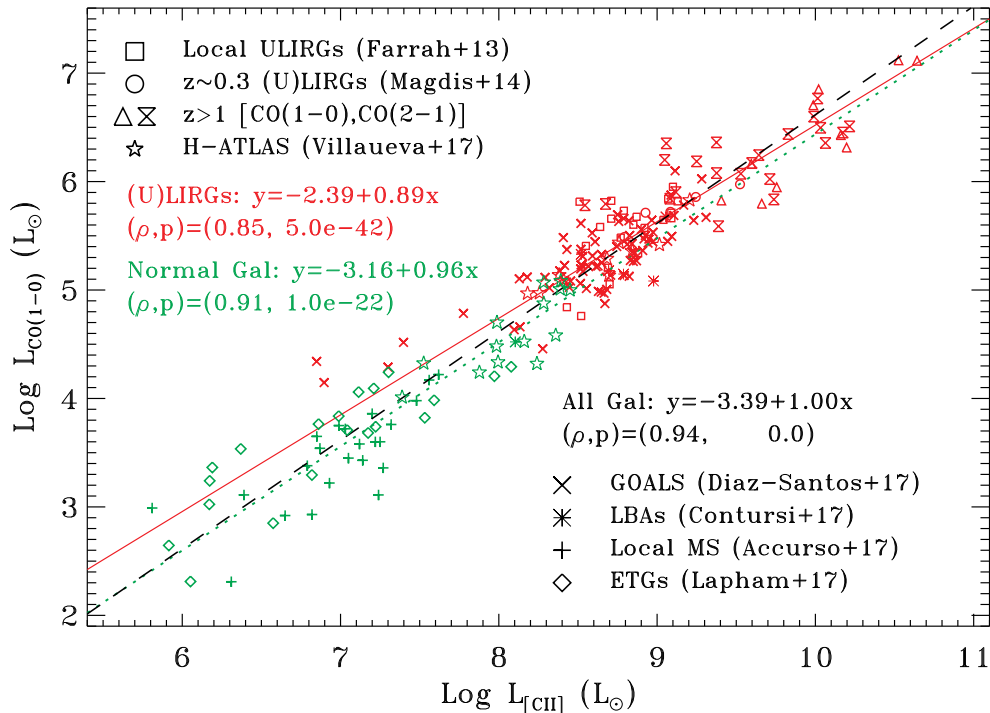


Figure 1. CO(1–0) line luminosity plotted against [C II] line luminosity. Red and green symbols show (U)LIRGs and normal galaxies, respectively. Open diamonds are early-type galaxies from Lapham et al. (2017), plus signs represent local main-sequence galaxies from Accurso et al. (2017b), asterisks demonstrate Lyman-break analogs at $z \sim 0.2$ from Contursi et al. (2017), crosses and squares respectively display local (U)LIRGs from Díaz-Santos et al. (2017) and Farrah et al. (2013), stars are the *H-ATLAS* star-forming sources at $z \sim 0.02 - 0.2$ from Ibar et al. (2015), circles show $z \sim 0.3$ (U)LIRGs from Magdis et al. (2014), triangles and bowties are high-redshift ($z > 1$) sources, including (U)LIRGs, QSOs and SMGs, respectively observed in CO(1–0) (Carilli & Walter 2013; Magdis et al. 2014; Rawle et al. 2014; Malhotra et al. 2001, 2017; Zhang et al. 2018b; Leung et al. 2019; Riechers et al. 2020), and in CO(2–1) (Carilli & Walter 2013; Ferkinhoff et al. 2014; Huynh et al. 2014; Pavesi et al. 2018, 2019; Cunningham et al. 2020; Riechers et al. 2020). The fitted trends are annotated with corresponding correlation coefficients (ρ) and probability of null hypothesis (p), and are plotted as red solid, green dotted and black dashed lines, for (U)LIRGs, normal galaxies and the whole sample, respectively.

recommended for determining the functional relationship between two parameters by Isobe et al. (1990), i.e.,

$$\log L_{\text{CO}}(L_{\odot}) = a + b \log L_{[\text{C II}]}(L_{\odot}), \quad (2)$$

The fitted trends are shown as red solid and green dotted lines in Figure 1, respectively for (U)LIRGs and normal galaxies. Using the same method, we also fitted the whole galaxy sample, and the obtained trend is plotted as the black dashed line in Figure 1.

Table 1 lists the number of objects in each sample, the fitting coefficients, 1σ errors, and scatters for the $L_{[\text{C II}]} - L_{\text{CO}(1-0)}$ relation. The intercepts shown in the table suggest that the CO(1–0) emission has a linear correlation with the [C II] emission. Furthermore, as shown in the middle panel of Figure 2, which plots the distributions of the logarithmic $L_{[\text{C II}]} - \text{to} - L_{\text{CO}(1-0)}$ ratios ($L_{[\text{C II}]} / L_{\text{CO}(1-0)}$) for different subsamples with various galaxy types/redshifts, we can see that the largest difference (a factor of ~ 1.6) of the mean $L_{[\text{C II}]} / L_{\text{CO}(1-0)}$

Table 1. Coefficients for Equations (2) and (3)

Sample	N	Intercept (a)	Slope (b)	Scatter (dex)
(U)LIRGs	148	$-2.39(0.34)$	$0.89(0.04)$	0.24
Normal	58	$-3.16(0.45)$	$0.96(0.06)$	0.29
All	206	$-3.39(0.21)$	$1.00(0.02)$	0.28

NOTE—Numbers in the parentheses give the 1σ uncertainties.

(indicated by the corresponding arrows) is between local (U)LIRGs (2500 ± 1300 ; red solid line) and MS galaxies (3900 ± 2700 ; green dash-dotted line). The (U)LIRG subsamples show a difference of $\lesssim 35$ per cent among the three redshift bins, with an increasing $L_{[\text{C II}]} / L_{\text{CO}(1-0)}$ ratio from $z = 0$ to $z > 1$ (3300 ± 2200). We also note that ETGs have a double-peaked distribution, much different from the other subsamples, but the

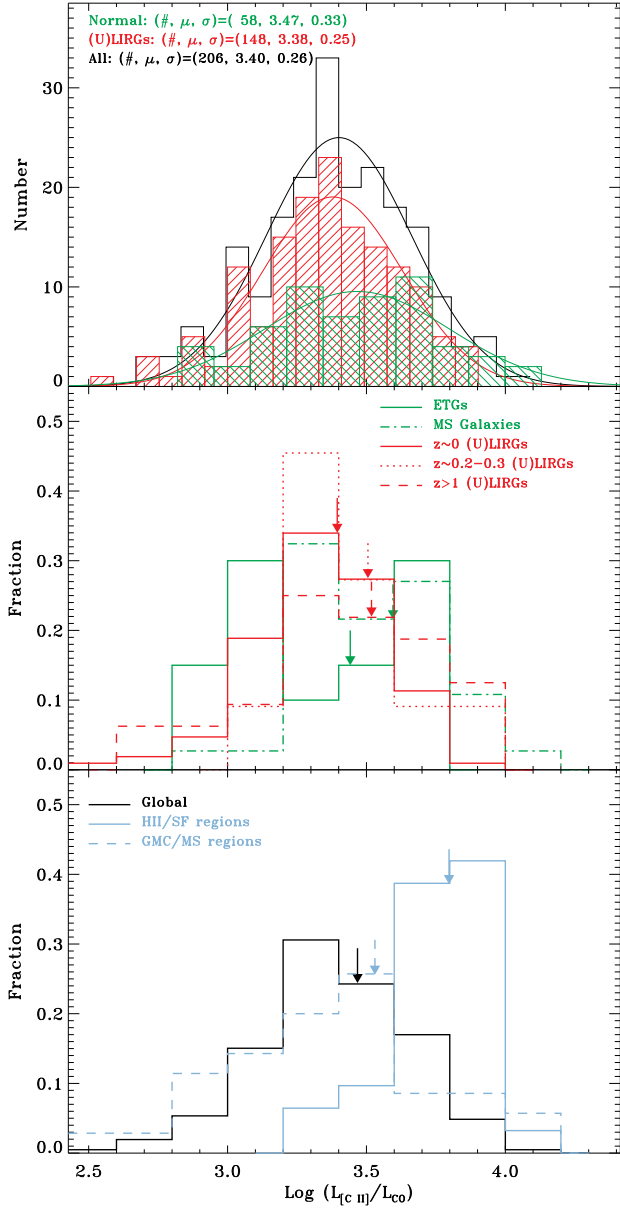


Figure 2. Comparison of the distribution of the [C II]-to-CO luminosity ratios for various samples. *Top:* The whole sample (black), (U)LIRGs (red) and normal galaxies (green), with the result of a Gaussian fit to the data superposed. The number of members, and mean $L_{[\text{C II}]} / L_{\text{CO}(1-0)}$ ratio and scatter from the Gaussian fit for each sample are also labelled with corresponding colors. *Middle:* ETGs (green solid line), MS galaxies (green dashed-dotted line), local (red solid line), $z \sim 0.2 - 0.3$ (red dotted line) and $z > 1$ (red dashed line) (U)LIRGs. *Bottom:* Galaxy-integrated results of our whole sample (black solid line), Galactic H II regions and extragalactic starburst nuclei (Stacey et al. 1991; blue solid line), and Galactic GMCs and non-starburst nuclei/regions (Stacey et al. 1991; Fadda et al. 2021; blue dashed line). The arrows in the middle and bottom panels indicate the corresponding mean values.

mean $L_{[\text{C II}]} / L_{\text{CO}(1-0)}$ ratio (2800 ± 1900) shows relatively small differences ($\lesssim 40\%$) compared with the other samples. Nevertheless, we caution that such analysis is possibly limited by the small numbers of the samples, especially for ETGs (20 members) and $z = 0.2 - 0.3$ (U)LIRGs (11 members).

As mentioned in Section 1 and already shown in Madden et al. (2020, and references therein), however, the situation changes much for dwarf/low-metallicity galaxies, most of which have $L_{[\text{C II}]} / L_{\text{CO}} \gtrsim 10^4$ (can be as high as $10^{4.9}$; also see Section 3.2), in general much larger than the ratios of massive/metal-rich galaxies. It is also interesting to see that, as demonstrated in the bottom panel of Figure 2, the [C II]-to-CO ratios on galaxy-wide scale (with a mean value of 2900 ± 1900) are more similar to those of Galactic giant molecular clouds (GMCs; Stacey et al. 1991) and non-starburst regions like NGC 7469 (Fadda et al. 2021), for which the mean ratio (3400 ± 3500) is ~ 2 times smaller than that (6300 ± 2400) of the Galactic H II regions and starburst nuclei presented in Stacey et al. (1991).

Our results indicate that, on galactic scale, massive/metal-rich galaxies under different physical conditions (from quiescent ETGs to extreme SF ULIRGs/SMGs) and at different redshifts (from $z = 0$ to $z \sim 6$) seem to share almost identical $L_{\text{CO}(1-0)} - L_{[\text{C II}]}$ relation, with comparable scatters of a factor $\lesssim 2$. The rms deviations of the data from the fitted relationships in $L_{\text{CO}(1-0)}$ are 0.24, 0.29 and 0.28 dex for (U)LIRGs, normal galaxies and the whole sample, respectively. We also note that the sources with CO(2-1)-converted $L_{\text{CO}(1-0)}$ have a larger scatter of 0.37 dex, confirming the additional uncertainty introduced by r_{21} as mentioned in Section 2.

Therefore, the CO(1-0) and [C II] emissions should have a strong physical connection as illustrated by both observational (e.g., Velusamy & Langer 2014; Pineda et al. 2017) and theoretical (Accurso et al. 2017a; Madden et al. 2020; Bisbas et al. 2021) works, even though the latter has additional origins other than PDRs. Given that the CO(1-0) emission is a commonly used tracer of M_{mol} , this scaling, established without any assumptions about the physical state of the gas, further confirms that the [C II] line is able to trace the total molecular gas for galaxies at local and high- z Universe. This is a powerful and particularly useful tool for probing the total molecular gas content in galaxies at $z > 4$ (e.g., Z18; Dessauges-Zavadsky et al. 2020), because that other tracers of molecular gas become increasingly difficult to observe with ground-based facilities, whereas the [C II] line is redshifted into the millimeter at-

mospheric windows accessible to ground (sub-)mm telescopes.

To convert the integrated luminosity of the [C II] line to the total molecular gas mass, we can utilize the $L_{\text{CO}(1-0)}-L_{[\text{C II}]}$ relations given by Equation (2), in combination with the CO-to-H₂ conversion factor, $\alpha_{\text{CO}}[M_{\odot} (\text{K km s}^{-1} \text{ pc}^2)^{-1}] \equiv M_{\text{mol}}/L'_{\text{CO}}$ (including a factor 1.36 to account for helium). Substituting $L_{\text{CO}(1-0)}$ in Equation (2) with Equation (1), we obtain the following $L_{[\text{C II}]}-M_{\text{mol}}$ relation,

$$\log M_{\text{mol}}(M_{\odot}) = \log(2.04 \times 10^4 \alpha_{\text{CO}}) + a + b \log L_{[\text{C II}]}(L_{\odot}). \quad (3)$$

Given the strong linear relation between $L_{\text{CO}(1-0)}$ and $L_{[\text{C II}]}$, alternatively, it is natural and convenient to define a [C II]-to-H₂ conversion factor by analogy with α_{CO} as in Z18, namely,

$$\alpha_{[\text{C II}]}(M_{\odot}/L_{\odot}) \equiv M_{\text{mol}}/L_{[\text{C II}]}. \quad (4)$$

By substituting Equation (1) and α_{CO} for M_{mol} , Equation (4) can be rewritten as,

$$\alpha_{[\text{C II}]} = 2.04 \times 10^4 \alpha_{\text{CO}} / (L_{[\text{C II}]} / L_{\text{CO}}). \quad (5)$$

To assess the value of $\alpha_{[\text{C II}]}$, we plot the distributions of the logarithmic $L_{[\text{C II}]}$ -to- $L_{\text{CO}(1-0)}$ ratios ($L_{[\text{C II}]} / L_{\text{CO}(1-0)}$) in the top panel of Figure 2 for the whole sample and the two subsamples, with the results of a Gaussian fit to the data superposed. The number of members, and the mean value and scatter from the Gaussian fit are also labelled. In general a normal distribution can well describe the observed $L_{[\text{C II}]} / L_{\text{CO}(1-0)}$ ratios. According to the results of the Gaussian fit shown in the top panel of Figure 2, $\alpha_{[\text{C II}]}$ is related with α_{CO} via,

$$\alpha_{[\text{C II}]} = [8.50, 6.91, 8.12] \times \alpha_{\text{CO}}. \quad (6)$$

for (U)LIRGs, normal galaxies and the whole sample, respectively. The corresponding uncertainties of $\alpha_{[\text{C II}]}$, caused by the scatter of $L_{[\text{C II}]} / L_{\text{CO}(1-0)}$, are 0.25 dex, 0.33 dex and 0.26 dex.

3.2. The choice of the CO-to-H₂ conversion factor

As shown in Equations (3) and (6), the conversion of $L_{[\text{C II}]}$ to M_{mol} relies entirely on the CO-to-H₂ conversion factor α_{CO} , in consequence of utilizing the CO emission to calibrate M_{mol} . However, the conversion factor of CO is a long and debated discussion in the literature. It can vary by a factor of 3–5, from 0.8–1.5 $M_{\odot} (\text{K km s}^{-1} \text{ pc}^2)^{-1}$ for extreme local and high- z starbursts like ULIRGs/SMGs (Downes & Solomon 1998)

Table 2. CO- and [C II]-to-H₂ Conversion Factors

Sample	α_{CO} ($M_{\odot} (\text{K km s}^{-1} \text{ pc}^2)^{-1}$)	$\alpha_{[\text{C II}]}$ (M_{\odot}/L_{\odot})	Uncertainty (dex)
(U)LIRGs	4.0	34.0	0.25
Normal	4.7	32.5	0.33
All	4.3	34.9	0.26

NOTE—(1) α_{CO} is adopted from Dunne et al. (2022). (2) The uncertainty of $\alpha_{[\text{C II}]}$ is estimated from the scatter of the $L_{[\text{C II}]} / L_{\text{CO}(1-0)}$ luminosity ratios.

to 4.36 $M_{\odot} (\text{K km s}^{-1} \text{ pc}^2)^{-1}$ for Milky Way-like galaxies (e.g., see Bolatto et al. 2013 for a review).

In recent years, however, an increasing number of studies, based on dust determinations and other molecular gas tracer such as [C I], have reported a lack of such bi-modality in α_{CO} (e.g., Magdis et al. 2012; Rowlands et al. 2014; Genzel et al. 2015; Dunne et al. 2022). Dunne et al. (2022) have estimated α_{CO} through a self-consistent cross-calibration between three different molecular gas tracers (i.e., CO, [C I] and sub-millimetre dust continuum) for a large, heterogeneous sample of galaxies up to $z \sim 6$. They find that the difference of α_{CO} between IR-luminous (i.e., $L_{\text{IR}} > 10^{11} L_{\odot}$) and less luminous ($L_{\text{IR}} < 10^{11} L_{\odot}$) galaxies is very small – around 10–20 per cent in the mean, rather than the often assumed factor of ~ 3 –5 as mentioned above. Our sample of galaxies, comprising different types of objects, demonstrates that they very likely share a universal $L_{[\text{C II}]}-L_{\text{CO}(1-0)}$ relation. Therefore, a bimodal α_{CO} would also lead to a bimodal [C II] conversion factor. However, a bimodal $\alpha_{[\text{C II}]}$ seems not supported by any observational evidence (e.g., Z18; Dessauges-Zavadsky et al. 2020) or by simulations (e.g., Madden et al. 2020; Vizgan et al. 2022) so far, and thus is unlikely applicable to our sample galaxies.

In light of the above considerations and given the appreciable overlap between our and Dunne et al. 2022's samples, we adopt the conversion factor α_{CO} of 4.0 and 4.7 $M_{\odot} (\text{K km s}^{-1} \text{ pc}^2)^{-1}$ (including the contribution of helium; their Table 7), respectively for (U)LIRGs and normal galaxies. For the whole sample, the mean value of 4.3 $M_{\odot} (\text{K km s}^{-1} \text{ pc}^2)^{-1}$ is used. Therefore, the corresponding $\alpha_{[\text{C II}]}$ are 34.0, 32.5 and 34.9 M_{\odot}/L_{\odot} , respectively for (U)LIRGs, normal galaxies and the whole sample (see Table 2). For ETGs only, we obtain $\alpha_{[\text{C II}], \text{ETG}}$ of 34.2 M_{\odot}/L_{\odot} with an uncertainty of 0.3 dex using the mean [C II]-to-CO ratio of 2800 ± 1900 given above and α_{CO} of 4.7 $M_{\odot} (\text{K km s}^{-1} \text{ pc}^2)^{-1}$, agreeing well with the other samples. Given the small differences

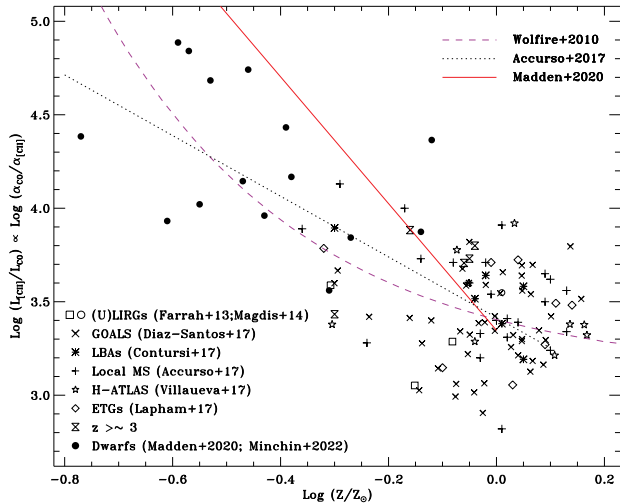


Figure 3. [C II]-to-CO luminosity ratio plotted versus metallicity for dwarf (Cormier et al. 2015; Grossi et al. 2016; Madden et al. 2020; Minchin et al. 2022) and massive galaxies. QSOs and AGNs are excluded from the plot. For comparison, the overplotted lines show α_{CO} as a function of metallicity from Wolfire et al. (2010, purple dashed line), Accurso et al. (2017b, black dotted line), and Madden et al. (2020, red solid line), assuming a constant $\alpha_{[\text{C II}]}$ of $34.9 M_{\odot}/L_{\odot}$.

(<10 per cent) between these samples, we conclude that $\alpha_{[\text{C II}]}$ is very likely universal, irrespective of galaxy types (e.g., intensity of star-forming activities, as already suggested by Z18) and redshifts.

Our derived $\alpha_{[\text{C II}]}$ are very similar to that ($31 M_{\odot}/L_{\odot}$) in Z18, though they have used a different approach to obtain the molecular gas mass (i.e., metallicity-dependent α_{CO} and KS relation). This is not unreasonable because the sample galaxies in Z18 are dominated by main-sequence (MS) objects. For *starbursts*, however, Z18 obtained $\alpha_{[\text{C II}]} = 22 M_{\odot}/L_{\odot}$ using a sample consisting of about 10 galaxies. Their value is $\sim 35\%$ smaller than our result for (U)LIRGs. This difference might be caused by the samples (our sample is larger by one order of magnitude; see Figure 8 in Z18) and CO conversion factors used between the two works (for these sources, Z18 adopted α_{CO} that has been derived for each source based their dynamical mass from Aravena et al. 2016).

Since Z18 sample includes dwarf galaxies with low metallicities, these results suggest that $\alpha_{[\text{C II}]}$ seems to be independent on metal abundance over the metallicity range ($12 + \log(\text{O}/\text{H}) = 7.9 - 8.9$) explored, as discussed in Z18. With a larger sample in hand, here we further investigate whether a metallicity-dependent α_{CO} and a constant $\alpha_{[\text{C II}]}$ can reproduce the observed $L_{[\text{C II}]} / L_{\text{CO}(1-0)}$ ratios. To this end, we plots $L_{[\text{C II}]} / L_{\text{CO}(1-0)}$, which is equal to $\alpha_{\text{CO}} / \alpha_{[\text{C II}]}$ accord-

ing to the definitions, as a function of Z , for the dwarf (Cormier et al. 2015; Grossi et al. 2016; Madden et al. 2020; Minchin et al. 2022) and our massive galaxies with metallicity measurements in Figure 3. For comparison, we also show the $\alpha_{\text{CO}}-Z$ relations from Wolfire et al. (2010, purple dashed line), Accurso et al. (2017b, black dotted line), and Madden et al. (2020, red solid line), assuming a constant $\alpha_{[\text{C II}]}$ of $34.9 M_{\odot}/L_{\odot}$.

As we can see from the figure, indeed, both the Wolfire et al. (2010) and Accurso et al. (2017b) relations, in combination with a constant $\alpha_{[\text{C II}]}$, follow the observed $L_{[\text{C II}]} / L_{\text{CO}(1-0)}-Z$ trend. However, the Madden et al. (2020) relation starts to over-predict the [C II]-to-CO ratio at $Z \sim 0.6Z_{\odot}$, which might be caused by their larger α_{CO} at lower metallicity. We can further check this by calculating mean $\alpha_{[\text{C II}]}$, which are 44 ± 33 and $58 \pm 69 M_{\odot}/L_{\odot}$, using the Z -dependent α_{CO} from Accurso et al. (2017b) and Madden et al. (2020), respectively, for our subsample with measured metallicities (excluding literature dwarf data; otherwise, the derived $\alpha_{\text{CO}} = 43 \pm 32$ and $87 \pm 169 M_{\odot}/L_{\odot}$, respectively). Therefore, it is difficult to draw a solid conclusion whether $\alpha_{[\text{C II}]}$ is insensitive to metallicity based on the current method and data set, due to the large uncertainty of α_{CO} for low- Z sources as already mentioned in §2.1.

3.3. Origin of the $L_{[\text{C II}]}-L_{\text{CO}(1-0)}$ relation

Given the multiple phases (ionized, neutral atomic and molecular) and powering sources (i.e., far-UV photons, cosmic rays, X-rays, turbulence and shocks; e.g. see a review in Wolfire et al. 2022) of the [C II] line, it is remarkable that there exists a linear correlation between the CO(1-0) and [C II] emissions. Therefore, it is intriguing to explore the reason(s) resulting in such a relation.

Using numerical simulations for star-forming, main-sequence galaxies at $z \sim 6$, Vizgan et al. (2022) ascribed this correlation ($M_{\text{mol}}-L_{[\text{C II}]}$; but sublinear in their work) to the KS law (Kennicutt 1998; also see Liu et al. 2015 for a sample including $2 \times$ more (U)LIRGs), a tight relationship between SFR and molecular gas mass. In fact, the powering source of the [C II] emission in star-forming galaxies should be dominated by the current SF activity (e.g., far-UV photons emitted by massive stars, SF-related cosmic rays and shocks; see, e.g., Stacey et al. 1985, 1991; Mookerjee et al. 2011), which is, in turn, correlated with the gas content of a galaxy.

However, our sample is a mixture of objects having (1) different levels of AGN activity; and (2) vastly varied SFEs: from low-SFE ETGs to extremely high-SFE ULIRGs. These gas-rich ETGs de-

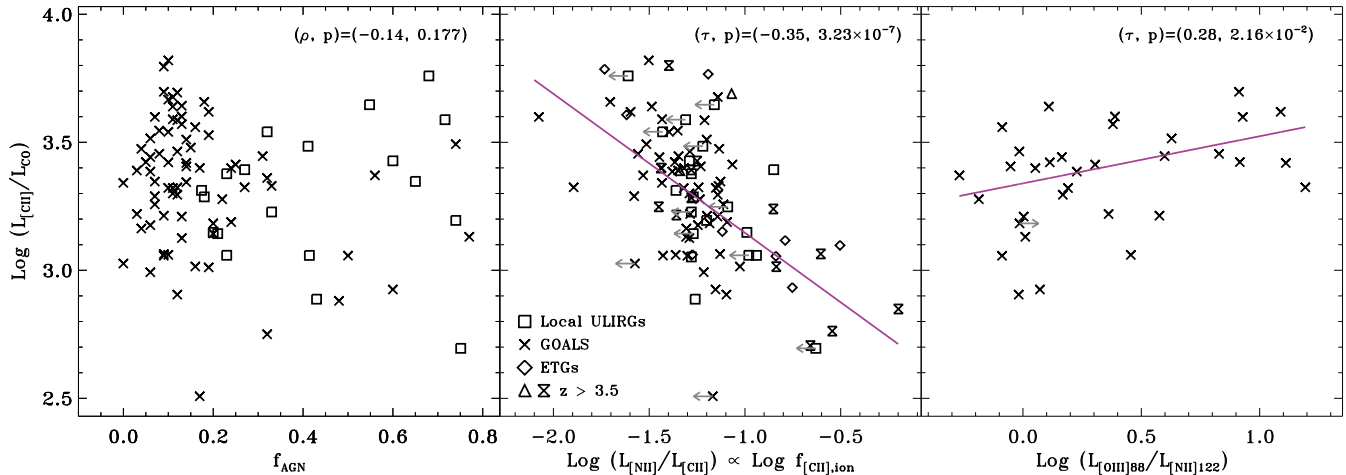


Figure 4. $L_{[\text{C II}]} / L_{\text{CO}(1-0)}$ plotted vs. f_{AGN} (left), $L_{[\text{N II}]205 \mu\text{m}} / L_{[\text{C II}]}$ (middle), and $[\text{O III}] 88 \mu\text{m}$ -to- $[\text{N II}] 122 \mu\text{m}$ flux ratio. Arrows in the middle and right panels respectively indicate upper and lower limits of the x -axis. The solid lines are linear fits to the data. The correlation coefficient and probability of null hypothesis are also given in each panel.

viate systematically from the KS relation (Davis et al. 2014), whereas ULIRGs have shown a well-known “[C II]/FIR” deficit, namely, their [C II]-to-FIR continuum luminosity ratios ($L_{[\text{C II}]} / L_{\text{FIR}}$) are smaller by as much as an order of magnitude compared to local less luminous galaxies (e.g., Malhotra et al. 2001; Luhman et al. 2003; Gullberg et al. 2015; Zhao et al. 2016a; Díaz-Santos et al. 2017). Furthermore, the [C II] emission in some ETGs is dominated by diffuse ionized gas (Lapham et al. 2017; Liu et al., in preparation), which might not relate to the current star-forming activity but is ionized by emission from old, hot stars such as postasymptotic giant branch stars (e.g. Binette et al. 1994). Therefore, it raises the question about whether the explanation in Vizgan et al. (2022) is also applicable to our results.

3.3.1. Where Does the [C II] Emission Come From?

To further investigate the origin of the $L_{[\text{C II}]} - L_{\text{CO}(1-0)}$ relation, first we explore the gas where the [C II] emission mainly arising from. To this end, firstly we plot the $L_{[\text{C II}]} / L_{\text{CO}(1-0)}$ ratio as a function of the potential contribution of an AGN to the bolometric luminosity (f_{AGN} ; see Díaz-Santos et al. 2017 for the calculation), as shown in the left panel of Figure 4, for the GOALS LIRGs and local ULIRGs. There is no correlation ($\rho = -0.14$ and $p = 0.177$) between these two parameters, suggesting that the [C II] emission in these sources is not dominated by the X-ray dissociation regions (XDRs). This argument is further evidenced by the fact that the $[\text{O I}] 63 \mu\text{m}$ -to-[C II] (non-ionized gas) luminosity ratios for almost all of these (U)LIRGs are less than unity (Farrah et al. 2013; Díaz-Santos et al. 2017), about an order of magnitude smaller than the values ($\gtrsim 10$; Meijerink et al. 2007) predicted by the XDR

models with an incident X-ray flux of $F_X(1-100 \text{ keV}) \approx 10 \text{ erg s}^{-1} \text{ cm}^{-2}$ (i.e., illuminated by a central source with the X-ray luminosity of $10^{43} \text{ erg s}^{-1}$ at a distance of 100 pc without extinction) and gas density of $n = 10^3 - 10^{6.5} \text{ cm}^{-3}$.

Secondly, we show $L_{[\text{C II}]} / L_{\text{CO}(1-0)}$ versus $L_{[\text{N II}]205 \mu\text{m}} / L_{[\text{C II}]}$, the observed [N II] 205 μm -to-[C II] luminosity ratio, which is a proxy of the [C II] fractional contribution of the ionized gas ($f_{[\text{C II}],\text{ion}}$; e.g., Oberst et al. 2006), in the middle panel of Figure 4 for those sources with available [N II] 205 μm measurements (De Breuck et al. 2014; Rawle et al. 2014; Pavesi et al. 2016, 2018, 2019; Zhao et al. 2016b; Cunningham et al. 2020; Litke et al. 2022). About ninety percent of these galaxies have their $L_{[\text{N II}]205 \mu\text{m}} / L_{[\text{C II}]}$ smaller than ~ 0.1 , suggesting $f_{[\text{C II}],\text{ion}} \lesssim 0.3$ using the carbon and nitrogen abundances in diffuse gas of the MilkyWay (Savage & Sembach 1996). Those ~ 10 galaxies having $L_{[\text{N II}]205 \mu\text{m}} / L_{[\text{C II}]} > 0.1$, however, do not show higher-but lower-than-average $L_{[\text{C II}]} / L_{\text{CO}(1-0)}$ ratios, and we will discuss this in more detail in §3.4.3. Our result indicates that the [C II] emission in the vast majority of our sample sources should not be dominated by the ionized gas.

Thirdly, we display $L_{[\text{C II}]} / L_{\text{CO}(1-0)}$ versus the $[\text{O III}] 88 \mu\text{m}$ -to- $[\text{N II}] 122 \mu\text{m}$ luminosity ratio ($L_{[\text{O III}]88 \mu\text{m}} / L_{[\text{N II}]122 \mu\text{m}}$) in the right panel of Figure 4, for the 33 GOALS LIRGs that have measured fluxes for both lines (Díaz-Santos et al. 2017). Since the ionization potentials of the [N II] 122 μm and [O III] 88 μm lines differ by more than a factor of two from 14.5 eV to 35 eV, and they have similar critical densities, the line ratio $L_{[\text{O III}]88 \mu\text{m}} / L_{[\text{N II}]122 \mu\text{m}}$ can be a good indicator of the hardness of the radiation field (e.g.,

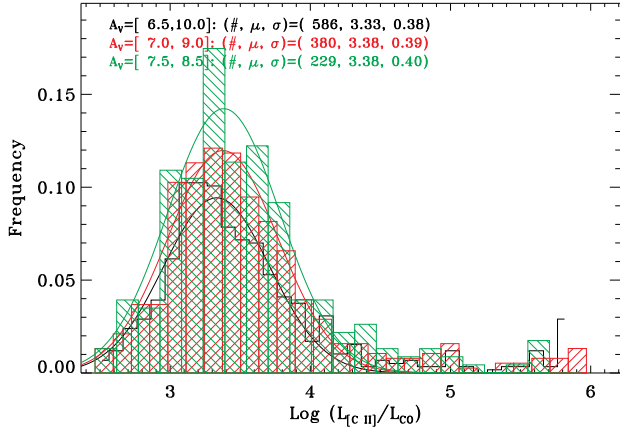


Figure 5. Distribution of $L_{[\text{C II}]} / L_{\text{CO}(1-0)}$ from Madden et al. (2020) PDR modelsets ($Z = 0.05 - 1 Z_{\odot}$, $G_0 = 10^{1.25} - 10^{4.06}$, and $n = 10^1 - 10^4 \text{ cm}^{-3}$), overlaid with the Gaussian fitting results. The black, red and green colors show the results of models having $A_V = 6.5 - 10$, $7 - 9$ and $7.5 - 8.5$ (all with mean $A_V \sim 8$), respectively.

Ferkinhoff et al. 2011; Zhang et al. 2018b) based on the Rubin (1985) H II models. As we can see from the figure, the Kendall’s τ correlation coefficient, computed using the *cenken* function in the *NADA* package within the public domain **R** statistical software environment¹, is $\tau = 0.28$, with a p -value of 2.2×10^{-2} , indicating that there only exists a very weak dependence (slope of 0.18) of $L_{[\text{C II}]} / L_{\text{CO}(1-0)}$ on $L_{[\text{O III}]}_{88 \mu\text{m}} / L_{[\text{N II}]}_{122 \mu\text{m}}$. This result further suggests that the [C II] emission should not mainly come from the ionized gas.

In summary, PDRs dominate the [C II] emission for the vast majority of our sample galaxies. However, the $L_{[\text{C II}]} - \text{SFR}$ relation has a much larger scatter of $0.4 - 0.6$ dex, both for simulated (e.g., Vallini et al. 2015; Vizgan et al. 2022) and observational data sets (e.g., De Looze et al. 2014; Z18; Vizgan et al. 2022), than that ($\lesssim 0.3$ dex) of the $L_{[\text{C II}]} - M_{\text{mol}}$ relation, indicating that $L_{[\text{C II}]}$ traces M_{mol} better than SFR (Z18). Therefore, it is very likely that the correlation between [C II] and CO emission is mainly caused by their co-spatial origins. However, it is still needed to answer why the relationship is almost linear and so tight over about five order of magnitude in CO(1–0) ([C II]) luminosity despite different physical conditions.

3.3.2. Comparison to PDR Models

In this section, we compare the observed line ratios with standard PDR models published in the literature. As it has been discussed in detail in Kaufman et al. (1999), Wolfire et al. (2010) and Madden et al. (2020),

the $L_{[\text{C II}]} / L_{\text{CO}(1-0)}$ ratio of a molecular cloud depends on gas density n , incident FUV radiation field G_0 , metallicity Z and column density N (and thus visual extinction A_V as $A_V \propto ZN$ assuming a linear relation between dust-to-gas ratio and metallicity; e.g., Kaufman et al. 1999; Wolfire et al. 2010). Furthermore, $L_{[\text{C II}]} / L_{\text{CO}(1-0)}$ is most sensitive to A_V (Wolfire et al. 2010; Madden et al. 2020).

Figure 5 plots the distributions of $L_{[\text{C II}]} / L_{\text{CO}(1-0)}$ adopted from the Madden et al. (2020) PDR modelset for different A_V ranges. For a given mean A_V of ~ 8 mag, which is the typical value of the Galaxy (e.g., Wolfire et al. 2010), the modelled $L_{[\text{C II}]} / L_{\text{CO}(1-0)}$ ratios show a log-normal distribution with a nearly constant mean value (μ) very close to our observed one, indicating that our sample galaxies may have an average A_V similar to the Galaxy. From the figure we can also see that the dispersion (σ) does not change with the range of A_V , and is a bit larger than the observed value, suggesting that it needs some other parameters to be responsible for the scatter of the observed $L_{[\text{C II}]} / L_{\text{CO}(1-0)}$ distribution.

The ratio of G_0 to n , G_0/n , an important parameter in the chemistry and physics of PDRs (Tielens & Hollenbach 1985), to a great extent determines the $L_{[\text{C II}]} / L_{\text{CO}(1-0)}$ ratio (e.g., Pak et al. 1998; Kaufman et al. 1999; Meijerink et al. 2007; Röllig et al. 2013) for fixed Z and fixed N (and thus fixed A_V). To explore whether the observed scatter can be attributed to the variation of G_0/n , we also compare the observed $L_{[\text{C II}]} / L_{\text{CO}(1-0)}$ to the PDR models computed with $Z = Z_{\odot}$ and much larger parameter space in G_0 and n in Figure 6. The left and right panels display the distributions of $L_{[\text{C II}]} / L_{\text{CO}(1-0)}$ for three different G_0/n ranges, adopted from the Wolfire–Kaufman “WK2020” (Pound & Wolfire 2023) and KOSMA-tau “kt2013wd01-7” clumpy (Röllig et al. 2013; Röllig & Ossenkopf-Okada 2022) modelsets², respectively. The “WK2020” modelset includes model grids computed with $G_0 = 10^{-0.5} - 10^{6.5}$ (in units of the Habing field of $1.6 \times 10^{-3} \text{ erg s}^{-1} \text{ cm}^{-2}$; Habing 1968), $n = 10^1 - 10^7 \text{ cm}^{-3}$, $Z = Z_{\odot}$, $A_V = 7$ mag, and a cosmic ray ionization rate of $\zeta_{\text{CR}} = 2 \times 10^{-16} \text{ s}^{-1}$ (Pound & Wolfire 2023) by assuming a plane-parallel geometry, and the “kt2013wd01-7” clumpy modelset contains models computed with $G_0 \sim 10^{0.2} - 10^{6.2}$, $n = 10^3 - 10^7 \text{ cm}^{-3}$, $Z = Z_{\odot}$, $\zeta_{\text{CR}} = 2 \times 10^{-16} \text{ s}^{-1}$, and maximum clump mass = $1000 M_{\odot}$ (which determines A_V) by using an ensemble of spherical clumps.

¹ <http://www.R-project.org/>

² PDRT Toolbox website: <https://dustem.astro.umd.edu>

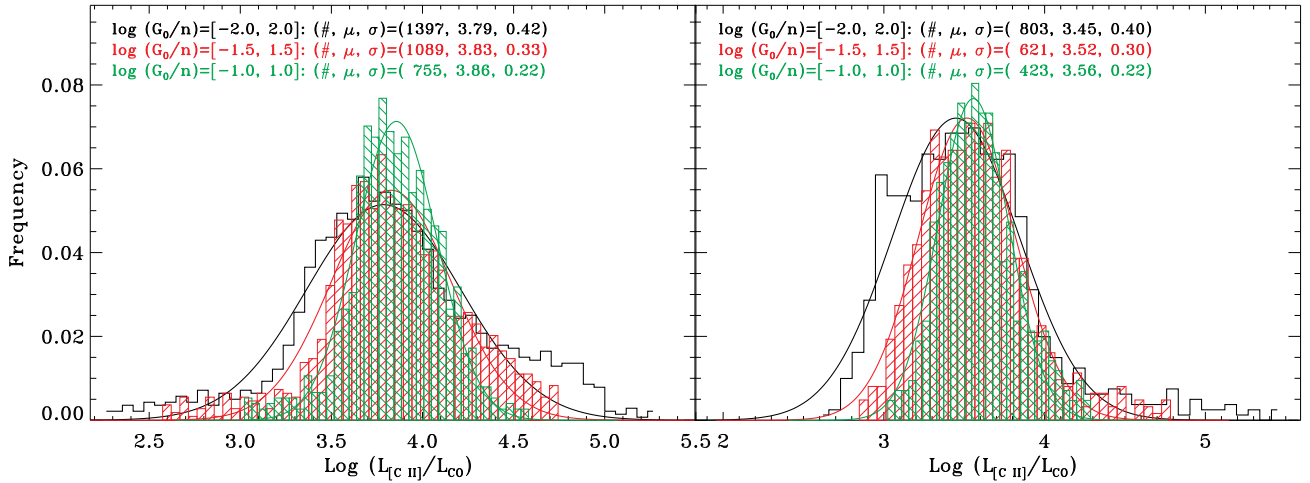


Figure 6. Distributions of $L_{[\text{C II}]} / L_{\text{CO}(1-0)}$ from the “WK2020” (left; Pound & Wolfire 2023) and “KOSMA-tau” (right; Röllig et al. 2013; Röllig & Ossenkopf-Okada 2022) PDR modelsets ($Z = Z_{\odot}$ and $\zeta_{\text{CR}} = 2 \times 10^{-16} \text{ s}^{-1}$), overlaid with the Gaussian fitting results. The black, red and green colors show the results of models having $G_0/n = 10^{-2} - 10^2$, $10^{-1.5} - 10^{1.5}$ and $10^{-1} - 10^1 \text{ cm}^3$, respectively.

Generally, the modelled $L_{[\text{C II}]} / L_{\text{CO}(1-0)}$ ratios also show a lognormal-like distribution. It can be seen from Figure 6 that the dispersion σ varies with the range of G_0/n considered. It increases from 0.2 dex to 0.4 dex as the G_0/n range changes from $10^{-1.0} - 10^{1.0}$ to $10^{-2.0} - 10^{2.0} \text{ cm}^3$ for both modelsets. Therefore, the gas conditions in the PDRs of different galaxies (with similar metallicities) can be largely varied, but variations in the resulted $L_{[\text{C II}]} / L_{\text{CO}(1-0)}$ ratio might be as small as 0.2–0.4 dex.

Compared to our sample presented in §3.1, we find that σ (~ 0.3 dex) from $G_0/n = 10^{-1.5} - 10^{1.5} \text{ cm}^3$ (red lines in Figure 6) is well consistent with the observed value. This is understandable since the derived G_0/n is usually in this range for local and high- z star-forming galaxies and AGNs/QSOs (e.g., Malhotra et al. 2001; Zhao et al. 2016a; Contursi et al. 2017; Díaz-Santos et al. 2017; Wardlow et al. 2017; Lapham & Young 2019; Rybak et al. 2020; Pensabene et al. 2021; Decarli et al. 2022). These results suggest that the tight and linear $L_{[\text{C II}]} - L_{\text{CO}(1-0)}$ relation could be a direct consequence of the effect that PDRs dominate the origin (and therefore the close physical association between the [C II] and CO emitting gas) of the [C II] emission.

3.4. Scatter of the $L_{[\text{C II}]} / L_{\text{CO}(1-0)}$ Ratio

3.4.1. Dependence of $L_{[\text{C II}]} / L_{\text{CO}(1-0)}$ on the IR Surface Brightness

As mentioned in §3.3, the $L_{[\text{C II}]} / L_{\text{FIR}}$ ratios of local ULIRGs may be smaller by as much as several $\times 10$ compared to local less luminous galaxies. This “[C II]/FIR” is found to correlate well with the total infrared lu-

minosity surface density (e.g., Díaz-Santos et al. 2017; Sutter & Fadda 2022), Σ_{IR} , which consists of both the energy injection and the compactness of a region, thereby traces the heating rate in the ISM. Therefore, it is necessary to check how the “[C II]/FIR” deficit will affect $L_{[\text{C II}]} / L_{\text{CO}(1-0)}$.

For our main sample, only a part of the GOALS LIRG and local ULIRG subsample galaxies have IR size measurements in Lutz et al. (2016), and thus for these sources we plot $L_{[\text{C II}]} / L_{\text{CO}(1-0)}$ as a function of Σ_{IR} ($\equiv \frac{L_{\text{IR}}}{2\pi r^2}$, where the radius r is estimated from the $70 \mu\text{m}$ images) in the bottom panel of Figure 7. Clearly, there exists a trend that $L_{[\text{C II}]} / L_{\text{CO}(1-0)}$ decreases as Σ_{IR} increases. To investigate this relation, we use the Kaplan–Meier estimate (Kaplan & Meier 1958) for censored data³. The resulting $L_{[\text{C II}]} / L_{\text{CO}(1-0)} - \Sigma_{\text{IR}}$, which has a steeper slope (about -0.3) when $\Sigma_{\text{IR}} \gtrsim 10^{11} L_{\odot} \text{ kpc}^{-2}$, is shown by the solid line in the figure, with a scatter of 0.19 dex in $L_{[\text{C II}]} / L_{\text{CO}(1-0)}$, reduced by $\sim 20\%$ compared with that (0.24 dex) of the original data. The trend might be caused by the following reasons:

(1) The deficit of the [C II] emission, for which there exist comprehensive studies (e.g., Malhotra et al. 2001; Luhman et al. 2003; Casey et al. 2014; Gullberg et al. 2015; Zhao et al. 2016a; Díaz-Santos et al. 2017; Rybak et al. 2019) and several explanations (e.g., see Casey et al. 2014 for a review; Muñoz & Oh 2016; Narayanan & Krumholz 2017; Bisbas et al. 2022; Liang et al. 2023) in the literature; and/or (2) a decreasing α_{CO} with increasing gas surface density (Σ_{gas}) when

³ Implemented in the *locfit.censor* function in the *locfit* package in R.

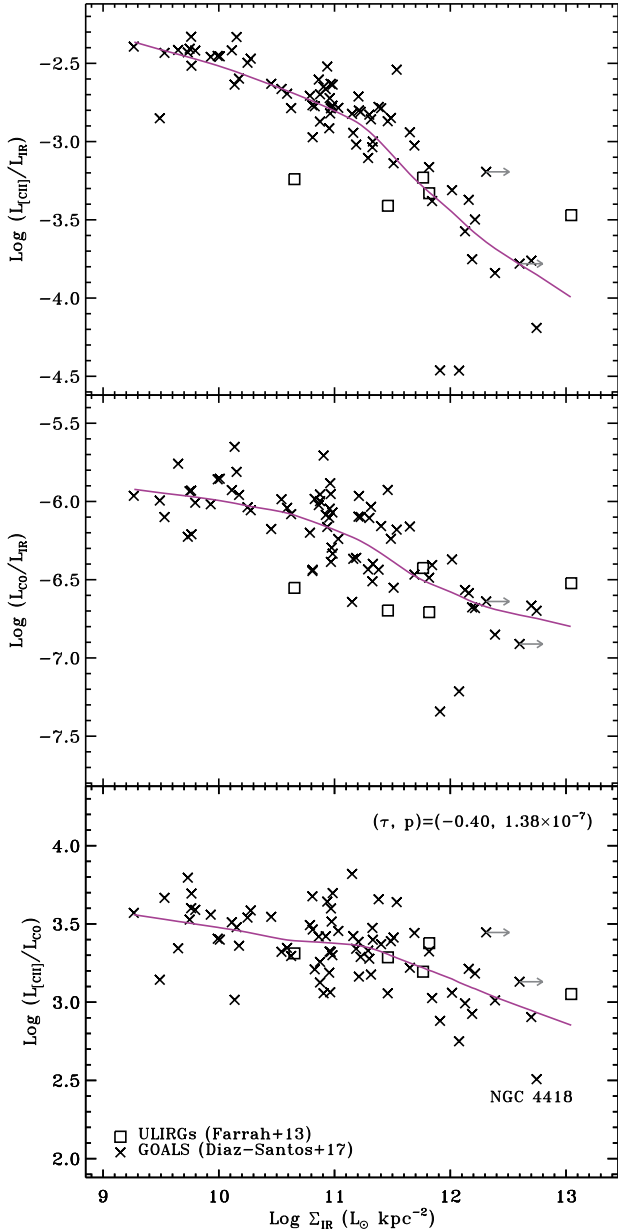


Figure 7. Infrared luminosity surface density Σ_{IR} plotted vs. $L_{[\text{CII}]} / L_{\text{IR}}$ (*top*), $L_{\text{CO}(1-0)} / L_{\text{IR}}$ (*middle*) and $L_{[\text{CII}]} / L_{\text{CO}(1-0)}$ (*bottom*). All the plots span 2.5 dex vertically for direct comparison. In each panel, arrows indicate lower limits of the x -axis, and the solid line shows the relation computed using the *locfit.censor* function. The correlation coefficient and probability of null hypothesis are also given in the bottom panel for the $L_{[\text{CII}]} / L_{\text{CO}(1-0)} - \Sigma_{\text{IR}}$ relation.

considering $\Sigma_{\text{IR}} \propto \Sigma_{\text{gas}}^N$ ($N \sim 1.4$; e.g., see Kennicutt 1998), as $L_{[\text{CII}]} / L_{\text{CO}} \propto \alpha_{\text{CO}} / \alpha_{[\text{CII}]}$.

The latter point seems to be well consistent with the prescription of $\alpha_{\text{CO}} \propto \Sigma_{\text{gas}}^{-0.5} \sim \Sigma_{\text{IR}}^{-0.35}$ for objects with similar metallicities as proposed in Bolatto et al. (2013). If this argument is true, it would suggest that $\alpha_{[\text{CII}]}$ al-

most does not vary with Σ_{IR} , and the $[\text{CII}]$ emission can serve an excellent molecular gas mass tracer for extreme starburst systems. As discussed in §3.2, however, it appears likely that the current cross-calibration of molecular gas mass tracers in metal-rich galaxies (Dunne et al. 2022) does not favour a significantly variable α_{CO} . For example, Arp 220 and NGC 4418, two of the most compact ($\Sigma_{\text{IR}} \sim 10^{12.7} L_{\odot} \text{ kpc}^{-2}$) starburst galaxies in our sample, have an averaged α_{CO} of 3.6 ± 0.5 and $4.4 \pm 0.7 M_{\odot} (\text{K km s}^{-1} \text{ pc}^2)^{-1}$ (Dunne et al. 2022), respectively.

Regarding the first point, we further explore it by plotting the $[\text{CII}]$ - and $\text{CO}(1-0)$ -to-IR luminosity ratios as a function of Σ_{IR} in the top and middle panels of Figure 7, respectively. Since all the three plots in Figure 7 span 2.5 dex vertically, we can make a direct comparison of the dependence on Σ_{IR} among different line-to-IR luminosity ratios. We can see that the $L_{[\text{CII}]} / L_{\text{IR}} - \Sigma_{\text{IR}}$ relation shows a steeper slope than $L_{\text{CO}(1-0)} / L_{\text{IR}} - \Sigma_{\text{IR}}$ (see also Valentino et al. 2020b for a similar trend in $L_{\text{CO}(1-0)} / L_{\text{IR}} - \Delta(\text{MS})$ relation), resulting in the dependence of $L_{[\text{CII}]} / L_{\text{CO}(1-0)}$ on Σ_{IR} . Therefore, the “[CII]/FIR” deficit is responsible for systematically decreasing in $L_{[\text{CII}]} / L_{\text{CO}(1-0)}$ with increasing Σ_{IR} .

According to the relation shown in the bottom panel of Figure 7, M_{mol} of those galaxies with $\Sigma_{\text{IR}} \gtrsim 10^{12} L_{\odot} \text{ kpc}^{-2}$ is likely to be systematically underestimated by a factor of $\gtrsim 2$ due to the deficit of the $[\text{CII}]$ emission. Furthermore, the total molecular gas mass can be underestimated by as much as about an order of magnitude for extreme cases like NGC 4418, though such systems are very rare (only 1 case) in our sample. In general, the dependence of $L_{[\text{CII}]} / L_{\text{CO}(1-0)}$ on Σ_{IR} only results in a small increase in the total scatter based on our sample.

3.4.2. Relation between $L_{[\text{CII}]} / L_{\text{CO}(1-0)}$ and Distance off Main Sequence

Employing a Bayesian analysis, Accurso et al. (2017b) find that the distance from the main sequence ($\equiv \Delta(\text{MS})$), which is related to the strength of UV radiation field, plays a secondary but statistically important role in determining the $L_{[\text{CII}]} / L_{\text{CO}(1-0)}$ ratio, in the sense that $L_{[\text{CII}]} / L_{\text{CO}(1-0)}$ monotonically increases with $\Delta(\text{MS})$ within the parameter space constrained ($-0.8 < \Delta(\text{MS}) < 1.3$). Here the distance off the main sequence is defined as:

$$\Delta(\text{MS}) = \log \frac{\text{sSFR}}{\text{sSFR}_{\text{MS}}} \quad (7)$$

where sSFR is the specific star formation rate (i.e., SFR / M_{\star}), and sSFR_{MS} the sSFR for main sequence galaxies, calculated with the same equation (adopted

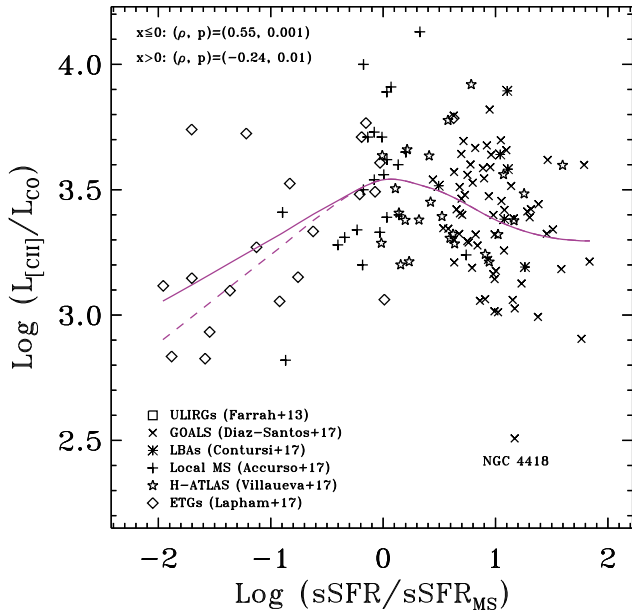


Figure 8. $L_{[\text{CII}]} / L_{\text{CO}(1-0)}$ plotted against $\text{sSFR} / \text{sSFR}_{\text{MS}}$. The solid purple line shows the relationship obtained with the *locfit* function using all data points, while the dashed line displays the relationship estimated by excluding the two apparent outliers (i.e., two ETGs with $\Delta(\text{MS}) < -1$ and $\log(L_{[\text{CII}]} / L_{\text{CO}}) > 3.7$). The correlation coefficient and probability of null hypothesis, computed separately for $\log(\text{sSFR} / \text{sSFR}_{\text{MS}}) \leq 0$ and $\log(\text{sSFR} / \text{sSFR}_{\text{MS}}) > 0$, are also given in the plot.

from Whitaker et al. 2012) in Accurso et al. (2017b). To further investigate the relation between $L_{[\text{CII}]} / L_{\text{CO}(1-0)}$ and $\Delta(\text{MS})$ for a larger dynamic range, we plot $L_{[\text{CII}]} / L_{\text{CO}(1-0)}$ as a function of $\Delta(\text{MS})$ in Figure 8, for the 138 objects with stellar mass measurements. Same as what found in Accurso et al. (2017b), indeed, $L_{[\text{CII}]} / L_{\text{CO}(1-0)}$ increases with $\Delta(\text{MS})$ when $-2 < \Delta(\text{MS}) \leq 0$, as illustrated by the solid purple line obtained with the *locfit* function in **R**. The Spearman correlation coefficient is $\rho = 0.55$, with the probability of null hypothesis $p = 0.001$, indicating a moderate positive correlation. If the two apparent outliers (i.e., two ETGs with $\Delta(\text{MS}) < -1$ and $\log(L_{[\text{CII}]} / L_{\text{CO}}) > 3.7$) are excluded from the fitting, an even stronger correlation can be obtained (as shown by the dashed line), with $\rho = 0.74$ and $p = 1.69 \times 10^{-6}$. This result suggests that M_{mol} could be systematically underestimated by a factor of 2–3 for galaxies with $\Delta(\text{MS}) \lesssim -1.5$.

When $0 < \Delta(\text{MS}) < 2$, by contrast, there only exists a very weak, negative ($\rho = -0.24$ and $p = 0.01$) correlation, indicating that $L_{[\text{CII}]} / L_{\text{CO}(1-0)}$ decreases slowly as $\Delta(\text{MS})$ increases. The difference between our and Accurso et al. (2017b) results is believed to be caused mainly by the samples used and the sam-

ple sizes, as Accurso et al. sample comprises 30 metal-rich and metal-poor galaxies, only eight out of which have $\Delta(\text{MS}) > 0.3$. Our results suggest that the $L_{[\text{CII}]} / L_{\text{CO}(1-0)}$ ratio is mainly determined by other physical parameter(s) for metal-rich, starburst systems.

3.4.3. Effect of the Contribution from Ionized Gas to the $[\text{CII}]$ Emission

In our analysis, the contribution from ionized gas to the $[\text{CII}]$ emission is not subtracted, and thus the molecular gas mass might be overestimated for the systems that the $[\text{CII}]$ emission is dominated by the ionized gas. To check whether this hypothesis is true, we plot the $L_{[\text{CII}]} / L_{\text{CO}(1-0)}$ ratio against the $L_{[\text{NII}]205\mu\text{m}} / L_{[\text{CII}]}$ ratio in the middle panel of Figure 4. As mentioned in §3.3.1, $L_{[\text{NII}]205\mu\text{m}} / L_{[\text{CII}]}$ can be used to estimate the fractional contribution ($f_{[\text{CII}],\text{ion}}$) from the diffuse ionized gas to the total $[\text{CII}]$ flux, namely $f_{[\text{CII}],\text{ion}} = \frac{[\text{CII}]_{\text{ion}}}{[\text{CII}]_{\text{total}}} = \left(\frac{[\text{CII}]}{[\text{NII}]}\right)_{\text{theo}} \times \left(\frac{[\text{NII}]}{[\text{CII}]}\right)_{\text{obs}}$, where $\left(\frac{[\text{CII}]}{[\text{NII}]}\right)_{\text{theo}}$ is the predicted $L_{[\text{CII}]} / L_{[\text{NII}]205\mu\text{m}}$ ratio in diffuse ionized gas. This is because that, $\left(\frac{[\text{CII}]}{[\text{NII}]}\right)_{\text{theo}}$ only shows a very weak dependence on electron density and temperature, and thus is almost constant for a given carbon-to-nitrogen abundance ratio (C/N; see, e.g., Oberst et al. 2006; Zhang et al. 2018b). We note that the C/N ratio in galaxies is nearly independent on metallicity, showing a dispersion of $\sigma = 0.20$ dex (Berg et al. 2019).

As demonstrated in the middle panel of Figure 4, there exist no obvious trend between these two ratios. The Kendall’s τ correlation coefficient, computed using the *cenken* function in the *NADA* package within **R**, is $\tau = -0.35$, with a p -value of 3.2×10^{-7} , indicating a weak anti-correlation between $L_{[\text{NII}]205\mu\text{m}} / L_{[\text{CII}]}$ and $L_{[\text{CII}]} / L_{\text{CO}(1-0)}$. This anti-correlation suggests that a larger $f_{[\text{CII}],\text{ion}}$ will lead to a lower $L_{[\text{CII}]} / L_{\text{CO}(1-0)}$ ratio, opposite to the aforementioned hypothesis that the contribution of ionized gas to the $[\text{CII}]$ emission would overestimate the total molecular gas mass. This result appears to be understandable in the sense that the lower the SF activity level is (as a consequence, a smaller G_0/n and thus lower $L_{[\text{CII}]} / L_{\text{CO}(1-0)}$), the higher the fractional contribution from the ionized gas is likely to happen (e.g., Díaz-Santos et al. 2017).

4. SUMMARY

In this paper we present the relation between the $[\text{CII}]$ line and the $\text{CO}(1-0)$ emission for a sample comprising about 200 local and high- z galaxies, including ETGs, main-sequence galaxies, (U)LIRGs/SMGs, and QSOs/AGNs. We explore the origin of this correlation, as well as investigate the dependence of the

[C II]-to-CO(1–0) luminosity ratio on different physical properties such as the IR luminosity surface density (Σ_{IR}), hardness of the UV radiation field ($[\text{O III}] 88 \mu\text{m}/[\text{N II}] 122 \mu\text{m}$), distance to the main sequence ($\Delta(\text{MS})$) and the fractional contribution of ionized gas ($[\text{N II}] 205 \mu\text{m}/[\text{C II}]$). We show that the [C II] emission can generally serve as a good tracer of the total molecular gas mass with an uncertainty of a factor of $\lesssim 2$. However, caution needs to be taken when applying a constant [C II]-to- M_{H_2} conversion factor to estimate the molecular gas content in some extreme cases. For galaxies having low-level SF activities (i.e., $\Delta(\text{MS}) \lesssim -1.5$) or high SFR surface density (i.e., $\Sigma_{\text{IR}} \gtrsim 10^{12} L_{\odot} \text{ kpc}^{-2}$), M_{mol} may be systematically underestimated by a factor of $\gtrsim 2$. Our main results are:

1. There exists a strong and tight (rms scatter $\lesssim 0.3$ dex), linear correlation between $L_{[\text{C II}]}$ and $L_{\text{CO}(1-0)}$ in massive galaxies located at different redshifts, i.e., $\log L_{\text{CO}} = (-3.39 \pm 0.21) + (1.00 \pm 0.02) \log L_{[\text{C II}]}$, confirming the [C II]’s capability to trace total molecular gas.
2. Based on the observed [C II]/CO(1–0) ratios and α_{CO} derived most recently (Dunne et al. 2022), we obtain the [C II]-to- M_{mol} conversion factor, $\alpha_{[\text{C II}]} = 34.9 M_{\odot}/L_{\odot}$ with an uncertainty of $\sigma = 0.26$ dex. There only exists a small difference between (U)LIRGs ($\alpha_{[\text{C II}]} = 34.0 M_{\odot}/L_{\odot}$, and $\sigma = 0.25$ dex) and less-luminous galaxies ($\alpha_{[\text{C II}]} = 32.5 M_{\odot}/L_{\odot}$ and $\sigma = 0.33$ dex) if they are analyzed separately.

3. By comparing the distributions between observed and modelled [C II]/CO(1–0) ratios, it is found that the tight and linear relation between [C II] and CO(1–0) is very likely determined by the range of G_0/n and average A_V in galaxies.
4. The [C II]/CO(1–0) ratio anti-correlates with Σ_{IR} for the subsample of local (U)LIRGs, and the relation becomes steeper when $\Sigma_{\text{IR}} \gtrsim 10^{11} L_{\odot} \text{ kpc}^{-2}$. The anti-correlation might be ascribed to the well-known deficit of [C II] in such kind of galaxies.
5. The [C II]/CO(1–0) ratio correlates positively with $\Delta(\text{MS})$ when $\Delta(\text{MS}) \lesssim 0$, and there is only a very weak, negative relation between these two parameters when $\Delta(\text{MS})$ becomes higher.
6. For systems in which the [C II] emission is dominated by ionized gas, the [C II]/CO(1–0) ratio tends to show a systematically smaller value, resulting in an underestimation of the total molecular gas.

- 1 We thank the anonymous referee for useful com-
- 2 ments/suggestions that significantly improved the pa-
- 3 per. YZ is grateful for support from the National Nat-
- 4 ural Science Foundation of China (NSFC) under grant
- 5 No. 12173079.

REFERENCES

- Accurso, G., Saintonge, A., Bisbas, T. G., & Viti, S. 2017a, MNRAS, 464, 3315, doi: [10.1093/mnras/stw2580](https://doi.org/10.1093/mnras/stw2580)
- Accurso, G., Saintonge, A., Catinella, B., et al. 2017b, MNRAS, 470, 4750, doi: [10.1093/mnras/stx1556](https://doi.org/10.1093/mnras/stx1556)
- Alatalo, K., Davis, T. A., Bureau, M., et al. 2013, MNRAS, 432, 1796, doi: [10.1093/mnras/sts299](https://doi.org/10.1093/mnras/sts299)
- Alloin, D., Barvainis, R., Gordon, M. A., & Antonucci, R. R. J. 1992, A&A, 265, 429
- Aravena, M., Hodge, J. A., Wagg, J., et al. 2014, MNRAS, 442, 558, doi: [10.1093/mnras/stu838](https://doi.org/10.1093/mnras/stu838)
- Aravena, M., Spilker, J. S., Bethermin, M., et al. 2016, MNRAS, 457, 4406, doi: [10.1093/mnras/stw275](https://doi.org/10.1093/mnras/stw275)
- Armus, L., Mazzarella, J. M., Evans, A. S., et al. 2009, PASP, 121, 559, doi: [10.1086/600092](https://doi.org/10.1086/600092)
- Asplund, M., Grevesse, N., Sauval, A. J., & Scott, P. 2009, ARA&A, 47, 481, doi: [10.1146/annurev.astro.46.060407.145222](https://doi.org/10.1146/annurev.astro.46.060407.145222)
- Bañados, E., Venemans, B. P., Mazzucchelli, C., et al. 2018, Nature, 553, 473, doi: [10.1038/nature25180](https://doi.org/10.1038/nature25180)
- Baan, W. A., Henkel, C., Loenen, A. F., Baudry, A., & Wiklind, T. 2008, A&A, 477, 747, doi: [10.1051/0004-6361:20077203](https://doi.org/10.1051/0004-6361:20077203)
- Bakx, T. J. L. C., Tamura, Y., Hashimoto, T., et al. 2020, MNRAS, 493, 4294, doi: [10.1093/mnras/staa509](https://doi.org/10.1093/mnras/staa509)
- Bell, E. F., McIntosh, D. H., Katz, N., & Weinberg, M. D. 2003, ApJS, 149, 289, doi: [10.1086/378847](https://doi.org/10.1086/378847)
- Berg, D. A., Erb, D. K., Henry, R. B. C., Skillman, E. D., & McQuinn, K. B. W. 2019, ApJ, 874, 93, doi: [10.3847/1538-4357/ab020a](https://doi.org/10.3847/1538-4357/ab020a)
- Binette, L., Magris, C. G., Stasińska, G., & Bruzual, A. G. 1994, A&A, 292, 13
- Bisbas, T. G., Tan, J. C., & Tanaka, K. E. I. 2021, MNRAS, 502, 2701, doi: [10.1093/mnras/stab121](https://doi.org/10.1093/mnras/stab121)

- Bisbas, T. G., Walch, S., Naab, T., et al. 2022, *ApJ*, 934, 115, doi: [10.3847/1538-4357/ac7960](https://doi.org/10.3847/1538-4357/ac7960)
- Bisbas, T. G., Zhang, Z.-Y., Gjergeric, E., et al. 2024, *MNRAS*, 527, 8886, doi: [10.1093/mnras/stad3782](https://doi.org/10.1093/mnras/stad3782)
- Bolatto, A. D., Wolfire, M., & Leroy, A. K. 2013, *ARA&A*, 51, 207, doi: [10.1146/annurev-astro-082812-140944](https://doi.org/10.1146/annurev-astro-082812-140944)
- Bothwell, M. S., Smail, I., Chapman, S. C., et al. 2013, *MNRAS*, 429, 3047, doi: [10.1093/mnras/sts562](https://doi.org/10.1093/mnras/sts562)
- Bouwens, R. J., Smit, R., Schouws, S., et al. 2022, *ApJ*, 931, 160, doi: [10.3847/1538-4357/ac5a4a](https://doi.org/10.3847/1538-4357/ac5a4a)
- Capak, P. L., Carilli, C., Jones, G., et al. 2015, *Nature*, 522, 455, doi: [10.1038/nature14500](https://doi.org/10.1038/nature14500)
- Cappellari, M., Emsellem, E., Krajnović, D., et al. 2011, *MNRAS*, 413, 813, doi: [10.1111/j.1365-2966.2010.18174.x](https://doi.org/10.1111/j.1365-2966.2010.18174.x)
- Carilli, C. L., & Walter, F. 2013, *ARA&A*, 51, 105, doi: [10.1146/annurev-astro-082812-140953](https://doi.org/10.1146/annurev-astro-082812-140953)
- Casey, C. M., Narayanan, D., & Cooray, A. 2014, *PhR*, 541, 45, doi: [10.1016/j.physrep.2014.02.009](https://doi.org/10.1016/j.physrep.2014.02.009)
- Casoli, F., Dickey, J., Kazes, I., et al. 1996, *A&AS*, 116, 193
- Cattorini, F., Gavazzi, G., Boselli, A., & Fossati, M. 2023, *A&A*, 671, A118, doi: [10.1051/0004-6361/202244738](https://doi.org/10.1051/0004-6361/202244738)
- Contursi, A., Baker, A. J., Berta, S., et al. 2017, *A&A*, 606, A86, doi: [10.1051/0004-6361/201730609](https://doi.org/10.1051/0004-6361/201730609)
- Cormier, D., Madden, S. C., Leboutteiller, V., et al. 2015, *A&A*, 578, A53, doi: [10.1051/0004-6361/201425207](https://doi.org/10.1051/0004-6361/201425207)
- Crocker, A. F., Bureau, M., Young, L. M., & Combes, F. 2011, *MNRAS*, 410, 1197, doi: [10.1111/j.1365-2966.2010.17537.x](https://doi.org/10.1111/j.1365-2966.2010.17537.x)
- Croxall, K. V., Smith, J. D., Pellegrini, E., et al. 2017, *ApJ*, 845, 96, doi: [10.3847/1538-4357/aa8035](https://doi.org/10.3847/1538-4357/aa8035)
- Cunningham, D. J. M., Chapman, S. C., Aravena, M., et al. 2020, *MNRAS*, 494, 4090, doi: [10.1093/mnras/staa820](https://doi.org/10.1093/mnras/staa820)
- da Cunha, E., Groves, B., Walter, F., et al. 2013, *ApJ*, 766, 13, doi: [10.1088/0004-637X/766/1/13](https://doi.org/10.1088/0004-637X/766/1/13)
- Davis, T. A., Young, L. M., Crocker, A. F., et al. 2014, *MNRAS*, 444, 3427, doi: [10.1093/mnras/stu570](https://doi.org/10.1093/mnras/stu570)
- De Breuck, C., Williams, R. J., Swinbank, M., et al. 2014, *A&A*, 565, A59, doi: [10.1051/0004-6361/201323331](https://doi.org/10.1051/0004-6361/201323331)
- De Looze, I., Cormier, D., Leboutteiller, V., et al. 2014, *A&A*, 568, A62, doi: [10.1051/0004-6361/201322489](https://doi.org/10.1051/0004-6361/201322489)
- De Vis, P., Jones, A., Viaene, S., et al. 2019, *A&A*, 623, A5, doi: [10.1051/0004-6361/201834444](https://doi.org/10.1051/0004-6361/201834444)
- Decarli, R., Walter, F., Carilli, C., et al. 2014, *ApJL*, 782, L17, doi: [10.1088/2041-8205/782/2/L17](https://doi.org/10.1088/2041-8205/782/2/L17)
- Decarli, R., Pensabene, A., Venemans, B., et al. 2022, *A&A*, 662, A60, doi: [10.1051/0004-6361/202142871](https://doi.org/10.1051/0004-6361/202142871)
- Dessauges-Zavadsky, M., Ginolfi, M., Pozzi, F., et al. 2020, *A&A*, 643, A5, doi: [10.1051/0004-6361/202038231](https://doi.org/10.1051/0004-6361/202038231)
- D'Eugenio, C., Daddi, E., Liu, D., & Gobat, R. 2023, *A&A*, 678, L9, doi: [10.1051/0004-6361/202347233](https://doi.org/10.1051/0004-6361/202347233)
- Díaz-Santos, T., Armus, L., Charmandaris, V., et al. 2017, *ApJ*, 846, 32, doi: [10.3847/1538-4357/aa81d7](https://doi.org/10.3847/1538-4357/aa81d7)
- Downes, D., & Solomon, P. M. 1998, *ApJ*, 507, 615, doi: [10.1086/306339](https://doi.org/10.1086/306339)
- Dunne, L., Maddox, S. J., Papadopoulos, P. P., Ivison, R. J., & Gomez, H. L. 2022, *MNRAS*, 517, 962, doi: [10.1093/mnras/stac2098](https://doi.org/10.1093/mnras/stac2098)
- Eales, S., Dunne, L., Clements, D., et al. 2010, *PASP*, 122, 499, doi: [10.1086/653086](https://doi.org/10.1086/653086)
- Fadda, D., Laine, S., & Appleton, P. N. 2021, *ApJ*, 909, 204, doi: [10.3847/1538-4357/abe0b8](https://doi.org/10.3847/1538-4357/abe0b8)
- Farrah, D., Leboutteiller, V., Spoon, H. W. W., et al. 2013, *ApJ*, 776, 38, doi: [10.1088/0004-637X/776/1/38](https://doi.org/10.1088/0004-637X/776/1/38)
- Ferkinhoff, C., Brisbin, D., Nikola, T., et al. 2015, *ApJ*, 806, 260, doi: [10.1088/0004-637X/806/2/260](https://doi.org/10.1088/0004-637X/806/2/260)
- . 2011, *ApJL*, 740, L29, doi: [10.1088/2041-8205/740/1/L29](https://doi.org/10.1088/2041-8205/740/1/L29)
- Ferkinhoff, C., Brisbin, D., Parshley, S., et al. 2014, *ApJ*, 780, 142, doi: [10.1088/0004-637X/780/2/142](https://doi.org/10.1088/0004-637X/780/2/142)
- Fernández-Ontiveros, J. A., Pérez-Montero, E., Vílchez, J. M., Amorín, R., & Spinoglio, L. 2021, *A&A*, 652, A23, doi: [10.1051/0004-6361/202039716](https://doi.org/10.1051/0004-6361/202039716)
- Ferrara, A., Vallini, L., Pallottini, A., et al. 2019, *MNRAS*, 489, 1, doi: [10.1093/mnras/stz2031](https://doi.org/10.1093/mnras/stz2031)
- Finkelstein, S. L., Papovich, C., Dickinson, M., et al. 2013, *Nature*, 502, 524, doi: [10.1038/nature12657](https://doi.org/10.1038/nature12657)
- Genzel, R., Tacconi, L. J., Lutz, D., et al. 2015, *ApJ*, 800, 20, doi: [10.1088/0004-637X/800/1/20](https://doi.org/10.1088/0004-637X/800/1/20)
- Glazer, K., Bradac, M., Sanders, R. L., et al. 2023, *arXiv e-prints*, arXiv:2309.11548, doi: [10.48550/arXiv.2309.11548](https://doi.org/10.48550/arXiv.2309.11548)
- Goldsmith, P. F., Langer, W. D., Pineda, J. L., & Velusamy, T. 2012, *ApJS*, 203, 13, doi: [10.1088/0067-0049/203/1/13](https://doi.org/10.1088/0067-0049/203/1/13)
- Griffith, E., Martini, P., & Conroy, C. 2019, *MNRAS*, 484, 562, doi: [10.1093/mnras/sty3405](https://doi.org/10.1093/mnras/sty3405)
- Grossi, M., Corbelli, E., Bizzocchi, L., et al. 2016, *A&A*, 590, A27, doi: [10.1051/0004-6361/201628123](https://doi.org/10.1051/0004-6361/201628123)
- Gullberg, B., De Breuck, C., Vieira, J. D., et al. 2015, *MNRAS*, 449, 2883, doi: [10.1093/mnras/stv372](https://doi.org/10.1093/mnras/stv372)
- Gururajan, G., Bethermin, M., Sulzenauer, N., et al. 2023, *A&A*, 676, A89, doi: [10.1051/0004-6361/202346449](https://doi.org/10.1051/0004-6361/202346449)
- Habing, H. J. 1968, *BAN*, 19, 421
- Hagimoto, M., Bakx, T. J. L. C., Serjeant, S., et al. 2023, *MNRAS*, 521, 5508, doi: [10.1093/mnras/stad784](https://doi.org/10.1093/mnras/stad784)
- Hainline, L. J., Blain, A. W., Smail, I., et al. 2011, *ApJ*, 740, 96, doi: [10.1088/0004-637X/740/2/96](https://doi.org/10.1088/0004-637X/740/2/96)
- Harrington, K. C., Weiss, A., Yun, M. S., et al. 2021, *ApJ*, 908, 95, doi: [10.3847/1538-4357/abcc01](https://doi.org/10.3847/1538-4357/abcc01)

- Heckman, T. M., Hoopes, C. G., Seibert, M., et al. 2005, *ApJL*, 619, L35, doi: [10.1086/425979](https://doi.org/10.1086/425979)
- Heintz, K. E., Watson, D., Oesch, P. A., Narayanan, D., & Madden, S. C. 2021, *ApJ*, 922, 147, doi: [10.3847/1538-4357/ac2231](https://doi.org/10.3847/1538-4357/ac2231)
- Herard-Demanche, T., Bouwens, R. J., Oesch, P. A., et al. 2023, arXiv e-prints, arXiv:2309.04525, doi: [10.48550/arXiv.2309.04525](https://doi.org/10.48550/arXiv.2309.04525)
- Herrera-Camus, R., Sturm, E., Graciá-Carpio, J., et al. 2018, *ApJ*, 861, 94, doi: [10.3847/1538-4357/aac0f6](https://doi.org/10.3847/1538-4357/aac0f6)
- Hinshaw, G., Weiland, J. L., Hill, R. S., et al. 2009, *ApJS*, 180, 225, doi: [10.1088/0067-0049/180/2/225](https://doi.org/10.1088/0067-0049/180/2/225)
- Hou, L. G., Han, J. L., Kong, M. Z., & Wu, X.-B. 2011, *ApJ*, 732, 72, doi: [10.1088/0004-637X/732/2/72](https://doi.org/10.1088/0004-637X/732/2/72)
- Howell, J. H., Armus, L., Mazzarella, J. M., et al. 2010, *ApJ*, 715, 572, doi: [10.1088/0004-637X/715/1/572](https://doi.org/10.1088/0004-637X/715/1/572)
- Hughes, T. M., Ibar, E., Villanueva, V., et al. 2017, *A&A*, 602, A49, doi: [10.1051/0004-6361/201629588](https://doi.org/10.1051/0004-6361/201629588)
- Huynh, M. T., Kimball, A. E., Norris, R. P., et al. 2014, *MNRAS*, 443, L54, doi: [10.1093/mnrasl/slu077](https://doi.org/10.1093/mnrasl/slu077)
- Hygate, A. P. S., Hodge, J. A., da Cunha, E., et al. 2023, *MNRAS*, 524, 1775, doi: [10.1093/mnras/stad1212](https://doi.org/10.1093/mnras/stad1212)
- Ibar, E., Lara-López, M. A., Herrera-Camus, R., et al. 2015, *MNRAS*, 449, 2498, doi: [10.1093/mnras/stv439](https://doi.org/10.1093/mnras/stv439)
- Isobe, T., Feigelson, E. D., Akritas, M. G., & Babu, G. J. 1990, *ApJ*, 364, 104, doi: [10.1086/169390](https://doi.org/10.1086/169390)
- Jiao, Q., Zhao, Y., Zhu, M., et al. 2017, *ApJL*, 840, L18, doi: [10.3847/2041-8213/aa6f0f](https://doi.org/10.3847/2041-8213/aa6f0f)
- Jiao, Q., Zhao, Y., Lu, N., et al. 2019, *ApJ*, 880, 133, doi: [10.3847/1538-4357/ab29ed](https://doi.org/10.3847/1538-4357/ab29ed)
- Kaplan, E. L., & Meier, P. 1958, *Journal of the American Statistical Association*, 53, 457, doi: [10.1080/01621459.1958.10501452](https://doi.org/10.1080/01621459.1958.10501452)
- Kaufman, M. J., Wolfire, M. G., Hollenbach, D. J., & Luhman, M. L. 1999, *ApJ*, 527, 795, doi: [10.1086/308102](https://doi.org/10.1086/308102)
- Kennicutt, Robert C., J. 1998, *ARA&A*, 36, 189, doi: [10.1146/annurev.astro.36.1.189](https://doi.org/10.1146/annurev.astro.36.1.189)
- Kewley, L. J., & Ellison, S. L. 2008, *ApJ*, 681, 1183, doi: [10.1086/587500](https://doi.org/10.1086/587500)
- Kilerci Eser, E., Goto, T., & Doi, Y. 2014, *ApJ*, 797, 54, doi: [10.1088/0004-637X/797/1/54](https://doi.org/10.1088/0004-637X/797/1/54)
- Kroupa, P. 2002, *Science*, 295, 82, doi: [10.1126/science.1067524](https://doi.org/10.1126/science.1067524)
- Lapham, R. C., & Young, L. M. 2019, *ApJ*, 875, 3, doi: [10.3847/1538-4357/ab0d23](https://doi.org/10.3847/1538-4357/ab0d23)
- Lapham, R. C., Young, L. M., & Crocker, A. 2017, *ApJ*, 840, 51, doi: [10.3847/1538-4357/aa6d83](https://doi.org/10.3847/1538-4357/aa6d83)
- Leung, T. K. D., Riechers, D. A., Baker, A. J., et al. 2019, *ApJ*, 871, 85, doi: [10.3847/1538-4357/aaf860](https://doi.org/10.3847/1538-4357/aaf860)
- Liang, L., Feldmann, R., Murray, N., et al. 2023, *MNRAS*, doi: [10.1093/mnras/stad3792](https://doi.org/10.1093/mnras/stad3792)
- Litke, K. C., Marrone, D. P., Aravena, M., et al. 2022, *ApJ*, 928, 179, doi: [10.3847/1538-4357/ac58f9](https://doi.org/10.3847/1538-4357/ac58f9)
- Liu, L., Gao, Y., & Greve, T. R. 2015, *ApJ*, 805, 31, doi: [10.1088/0004-637X/805/1/31](https://doi.org/10.1088/0004-637X/805/1/31)
- Lo, N., Cunningham, M. R., Jones, P. A., et al. 2014, *ApJL*, 797, L17, doi: [10.1088/2041-8205/797/2/L17](https://doi.org/10.1088/2041-8205/797/2/L17)
- Lu, N., Zhao, Y., Xu, C. K., et al. 2015, *ApJL*, 802, L11, doi: [10.1088/2041-8205/802/1/L11](https://doi.org/10.1088/2041-8205/802/1/L11)
- Lu, N., Zhao, Y., Díaz-Santos, T., et al. 2017, *ApJS*, 230, 1, doi: [10.3847/1538-4365/aa6476](https://doi.org/10.3847/1538-4365/aa6476)
- Luhman, M. L., Satyapal, S., Fischer, J., et al. 2003, *ApJ*, 594, 758, doi: [10.1086/376965](https://doi.org/10.1086/376965)
- Lutz, D., Berta, S., Contursi, A., et al. 2016, *A&A*, 591, A136, doi: [10.1051/0004-6361/201527706](https://doi.org/10.1051/0004-6361/201527706)
- Madden, S. C., Cormier, D., Hony, S., et al. 2020, *A&A*, 643, A141, doi: [10.1051/0004-6361/202038860](https://doi.org/10.1051/0004-6361/202038860)
- Magdis, G. E., Daddi, E., Béthermin, M., et al. 2012, *ApJ*, 760, 6, doi: [10.1088/0004-637X/760/1/6](https://doi.org/10.1088/0004-637X/760/1/6)
- Magdis, G. E., Rigopoulou, D., Hopwood, R., et al. 2014, *ApJ*, 796, 63, doi: [10.1088/0004-637X/796/1/63](https://doi.org/10.1088/0004-637X/796/1/63)
- Malhotra, S., Kaufman, M. J., Hollenbach, D., et al. 2001, *ApJ*, 561, 766, doi: [10.1086/323046](https://doi.org/10.1086/323046)
- Malhotra, S., Rhoads, J. E., Finkelstein, K., et al. 2017, *ApJ*, 835, 110, doi: [10.3847/1538-4357/835/1/110](https://doi.org/10.3847/1538-4357/835/1/110)
- Maragkoudakis, A., Zezas, A., Ashby, M. L. N., & Willner, S. P. 2018, *MNRAS*, 475, 1485, doi: [10.1093/mnras/stx3247](https://doi.org/10.1093/mnras/stx3247)
- Meijerink, R., Spaans, M., & Israel, F. P. 2007, *A&A*, 461, 793, doi: [10.1051/0004-6361:20066130](https://doi.org/10.1051/0004-6361:20066130)
- Michałowski, M. J., Dunlop, J. S., Cirasuolo, M., et al. 2012, *A&A*, 541, A85, doi: [10.1051/0004-6361/201016308](https://doi.org/10.1051/0004-6361/201016308)
- Michiyama, T., Ueda, J., Tadaki, K.-i., et al. 2020, *ApJL*, 897, L19, doi: [10.3847/2041-8213/ab9d28](https://doi.org/10.3847/2041-8213/ab9d28)
- Michiyama, T., Saito, T., Tadaki, K.-i., et al. 2021, *ApJS*, 257, 28, doi: [10.3847/1538-4365/ac16df](https://doi.org/10.3847/1538-4365/ac16df)
- Minchin, R., Fadda, D., Taylor, R., Deshev, B., & Davies, J. 2022, *AJ*, 164, 44, doi: [10.3847/1538-3881/ac746d](https://doi.org/10.3847/1538-3881/ac746d)
- Mirabel, I. F., Booth, R. S., Garay, G., Johansson, L. E. B., & Sanders, D. B. 1990, *A&A*, 236, 327
- Montoya Arroyave, I., Cicone, C., Makrolevaditi, E., et al. 2023, *A&A*, 673, A13, doi: [10.1051/0004-6361/202245046](https://doi.org/10.1051/0004-6361/202245046)
- Mookerjea, B., Kramer, C., Buchbender, C., et al. 2011, *A&A*, 532, A152, doi: [10.1051/0004-6361/201116447](https://doi.org/10.1051/0004-6361/201116447)
- Moustakas, J., & Kennicutt, Robert C., J. 2006, *ApJS*, 164, 81, doi: [10.1086/500971](https://doi.org/10.1086/500971)
- Muñoz, J. A., & Oh, S. P. 2016, *MNRAS*, 463, 2085, doi: [10.1093/mnras/stw2102](https://doi.org/10.1093/mnras/stw2102)

- Narayanan, D., & Krumholz, M. R. 2017, *MNRAS*, 467, 50, doi: [10.1093/mnras/stw3218](https://doi.org/10.1093/mnras/stw3218)
- Oberst, T. E., Parshley, S. C., Stacey, G. J., et al. 2006, *ApJL*, 652, L125, doi: [10.1086/510289](https://doi.org/10.1086/510289)
- Offner, S. S. R., Bisbas, T. G., Bell, T. A., & Viti, S. 2014, *MNRAS*, 440, L81, doi: [10.1093/mnrasl/slu013](https://doi.org/10.1093/mnrasl/slu013)
- Overzier, R. A., Heckman, T. M., Tremonti, C., et al. 2009, *ApJ*, 706, 203, doi: [10.1088/0004-637X/706/1/203](https://doi.org/10.1088/0004-637X/706/1/203)
- Pak, S., Jaffe, D. T., van Dishoeck, E. F., Johansson, L. E. B., & Booth, R. S. 1998, *ApJ*, 498, 735, doi: [10.1086/305584](https://doi.org/10.1086/305584)
- Papadopoulos, P., Dunne, L., & Maddox, S. 2022, *MNRAS*, 510, 725, doi: [10.1093/mnras/stab3194](https://doi.org/10.1093/mnras/stab3194)
- Papadopoulos, P. P., & Greve, T. R. 2004, *ApJL*, 615, L29, doi: [10.1086/426059](https://doi.org/10.1086/426059)
- Pavesi, R., Riechers, D. A., Faisst, A. L., Stacey, G. J., & Capak, P. L. 2019, *ApJ*, 882, 168, doi: [10.3847/1538-4357/ab3a46](https://doi.org/10.3847/1538-4357/ab3a46)
- Pavesi, R., Riechers, D. A., Capak, P. L., et al. 2016, *ApJ*, 832, 151, doi: [10.3847/0004-637X/832/2/151](https://doi.org/10.3847/0004-637X/832/2/151)
- Pavesi, R., Riechers, D. A., Sharon, C. E., et al. 2018, *ApJ*, 861, 43, doi: [10.3847/1538-4357/aac6b6](https://doi.org/10.3847/1538-4357/aac6b6)
- Pensabene, A., Decarli, R., Bañados, E., et al. 2021, *A&A*, 652, A66, doi: [10.1051/0004-6361/202039696](https://doi.org/10.1051/0004-6361/202039696)
- Pereira-Santaella, M., Rigopoulou, D., Magdis, G. E., et al. 2019, *MNRAS*, 486, 5621, doi: [10.1093/mnras/stz1218](https://doi.org/10.1093/mnras/stz1218)
- Pérez-Díaz, B., Pérez-Montero, E., Fernández-Ontiveros, J. A., Vílchez, J. M., & Amorín, R. 2024, *Nature Astronomy*, 8, 368, doi: [10.1038/s41550-023-02171-x](https://doi.org/10.1038/s41550-023-02171-x)
- Pettini, M., & Pagel, B. E. J. 2004, *MNRAS*, 348, L59, doi: [10.1111/j.1365-2966.2004.07591.x](https://doi.org/10.1111/j.1365-2966.2004.07591.x)
- Pineda, J. L., Langer, W. D., Goldsmith, P. F., et al. 2017, *ApJ*, 839, 107, doi: [10.3847/1538-4357/aa683a](https://doi.org/10.3847/1538-4357/aa683a)
- Pound, M. W., & Wolfire, M. G. 2023, *AJ*, 165, 25, doi: [10.3847/1538-3881/ac9b1f](https://doi.org/10.3847/1538-3881/ac9b1f)
- Rawle, T. D., Egami, E., Busmann, R. S., et al. 2014, *ApJ*, 783, 59, doi: [10.1088/0004-637X/783/1/59](https://doi.org/10.1088/0004-637X/783/1/59)
- Reuter, C., Spilker, J. S., Vieira, J. D., et al. 2023, *ApJ*, 948, 44, doi: [10.3847/1538-4357/acaf51](https://doi.org/10.3847/1538-4357/acaf51)
- Riechers, D. A., Hodge, J. A., Pavesi, R., et al. 2020, *ApJ*, 895, 81, doi: [10.3847/1538-4357/ab8c48](https://doi.org/10.3847/1538-4357/ab8c48)
- Rigopoulou, D., Pereira-Santaella, M., Magdis, G. E., et al. 2018, *MNRAS*, 473, 20, doi: [10.1093/mnras/stx2311](https://doi.org/10.1093/mnras/stx2311)
- Röllig, M., & Ossenkopf-Okada, V. 2022, *A&A*, 664, A67, doi: [10.1051/0004-6361/202141854](https://doi.org/10.1051/0004-6361/202141854)
- Röllig, M., Szczerba, R., Ossenkopf, V., & Glück, C. 2013, *A&A*, 549, A85, doi: [10.1051/0004-6361/201118190](https://doi.org/10.1051/0004-6361/201118190)
- Rowlands, K., Dunne, L., Dye, S., et al. 2014, *MNRAS*, 441, 1017, doi: [10.1093/mnras/stu510](https://doi.org/10.1093/mnras/stu510)
- Rubin, R. H. 1985, *ApJS*, 57, 349, doi: [10.1086/191007](https://doi.org/10.1086/191007)
- Rupke, D. S. N., Veilleux, S., & Baker, A. J. 2008, *ApJ*, 674, 172, doi: [10.1086/522363](https://doi.org/10.1086/522363)
- Rybak, M., Zavala, J. A., Hodge, J. A., Casey, C. M., & Werf, P. v. d. 2020, *ApJL*, 889, L11, doi: [10.3847/2041-8213/ab63de](https://doi.org/10.3847/2041-8213/ab63de)
- Rybak, M., Calistro Rivera, G., Hodge, J. A., et al. 2019, *ApJ*, 876, 112, doi: [10.3847/1538-4357/ab0e0f](https://doi.org/10.3847/1538-4357/ab0e0f)
- Rybak, M., van Marrewijk, J., Hodge, J. A., et al. 2023, *A&A*, 679, A119, doi: [10.1051/0004-6361/202347315](https://doi.org/10.1051/0004-6361/202347315)
- Sanders, D. B., & Mirabel, I. F. 1996, *ARA&A*, 34, 749, doi: [10.1146/annurev.astro.34.1.749](https://doi.org/10.1146/annurev.astro.34.1.749)
- Sanders, R. L., Shapley, A. E., Jones, T., et al. 2023, *ApJ*, 942, 24, doi: [10.3847/1538-4357/aca46f](https://doi.org/10.3847/1538-4357/aca46f)
- Santini, P., Maiolino, R., Magnelli, B., et al. 2010, *A&A*, 518, L154, doi: [10.1051/0004-6361/201014748](https://doi.org/10.1051/0004-6361/201014748)
- Sargent, M. T., Daddi, E., Béthermin, M., et al. 2014, *ApJ*, 793, 19, doi: [10.1088/0004-637X/793/1/19](https://doi.org/10.1088/0004-637X/793/1/19)
- Savage, B. D., & Sembach, K. R. 1996, *ARA&A*, 34, 279, doi: [10.1146/annurev.astro.34.1.279](https://doi.org/10.1146/annurev.astro.34.1.279)
- Schouws, S., Bouwens, R., Smit, R., et al. 2023, *ApJ*, 954, 103, doi: [10.3847/1538-4357/ace10c](https://doi.org/10.3847/1538-4357/ace10c)
- Scoville, N., Aussel, H., Sheth, K., et al. 2014, *ApJ*, 783, 84, doi: [10.1088/0004-637X/783/2/84](https://doi.org/10.1088/0004-637X/783/2/84)
- Scoville, N., Sheth, K., Aussel, H., et al. 2016, *ApJ*, 820, 83, doi: [10.3847/0004-637X/820/2/83](https://doi.org/10.3847/0004-637X/820/2/83)
- Shi, Y., Wang, J., Zhang, Z.-Y., et al. 2015, *ApJL*, 804, L11, doi: [10.1088/2041-8205/804/1/L11](https://doi.org/10.1088/2041-8205/804/1/L11)
- Solomon, P. M., Downes, D., Radford, S. J. E., & Barrett, J. W. 1997, *ApJ*, 478, 144, doi: [10.1086/303765](https://doi.org/10.1086/303765)
- Solomon, P. M., & Vanden Bout, P. A. 2005, *ARA&A*, 43, 677, doi: [10.1146/annurev.astro.43.051804.102221](https://doi.org/10.1146/annurev.astro.43.051804.102221)
- Sommovigo, L., Ferrara, A., Carniani, S., et al. 2021, *MNRAS*, 503, 4878, doi: [10.1093/mnras/stab720](https://doi.org/10.1093/mnras/stab720)
- Spilker, J. S., Marrone, D. P., Aguirre, J. E., et al. 2014, *ApJ*, 785, 149, doi: [10.1088/0004-637X/785/2/149](https://doi.org/10.1088/0004-637X/785/2/149)
- Stacey, G. J., Geis, N., Genzel, R., et al. 1991, *ApJ*, 373, 423, doi: [10.1086/170062](https://doi.org/10.1086/170062)
- Stacey, G. J., Hailey-Dunsheath, S., Ferkinhoff, C., et al. 2010, *ApJ*, 724, 957, doi: [10.1088/0004-637X/724/2/957](https://doi.org/10.1088/0004-637X/724/2/957)
- Stacey, G. J., Viscuso, P. J., Fuller, C. E., & Kurtz, N. T. 1985, *ApJ*, 289, 803, doi: [10.1086/162944](https://doi.org/10.1086/162944)
- Sun, F., Helton, J. M., Egami, E., et al. 2024, *ApJ*, 961, 69, doi: [10.3847/1538-4357/ad07e3](https://doi.org/10.3847/1538-4357/ad07e3)
- Sutter, J., & Fadda, D. 2022, *ApJ*, 926, 82, doi: [10.3847/1538-4357/ac4252](https://doi.org/10.3847/1538-4357/ac4252)
- Thomson, A. P., Ivison, R. J., Smail, I., et al. 2012, *MNRAS*, 425, 2203, doi: [10.1111/j.1365-2966.2012.21584.x](https://doi.org/10.1111/j.1365-2966.2012.21584.x)
- Tielens, A. G. G. M., & Hollenbach, D. 1985, *ApJ*, 291, 722, doi: [10.1086/163111](https://doi.org/10.1086/163111)

- Tremonti, C. A., Heckman, T. M., Kauffmann, G., et al. 2004, *ApJ*, 613, 898, doi: [10.1086/423264](https://doi.org/10.1086/423264)
- U, V., Sanders, D. B., Mazzarella, J. M., et al. 2012, *ApJS*, 203, 9, doi: [10.1088/0067-0049/203/1/9](https://doi.org/10.1088/0067-0049/203/1/9)
- Urquhart, S. A., Bendo, G. J., Serjeant, S., et al. 2022, *MNRAS*, 511, 3017, doi: [10.1093/mnras/stac150](https://doi.org/10.1093/mnras/stac150)
- Valentino, F., Magdis, G. E., Daddi, E., et al. 2018, *ApJ*, 869, 27, doi: [10.3847/1538-4357/aaeb88](https://doi.org/10.3847/1538-4357/aaeb88)
- . 2020a, *ApJ*, 890, 24, doi: [10.3847/1538-4357/ab6603](https://doi.org/10.3847/1538-4357/ab6603)
- Valentino, F., Daddi, E., Puglisi, A., et al. 2020b, *A&A*, 641, A155, doi: [10.1051/0004-6361/202038322](https://doi.org/10.1051/0004-6361/202038322)
- Vallini, L., Gallerani, S., Ferrara, A., Pallottini, A., & Yue, B. 2015, *ApJ*, 813, 36, doi: [10.1088/0004-637X/813/1/36](https://doi.org/10.1088/0004-637X/813/1/36)
- Velusamy, T., & Langer, W. D. 2014, *A&A*, 572, A45, doi: [10.1051/0004-6361/201424350](https://doi.org/10.1051/0004-6361/201424350)
- Venemans, B. P., Walter, F., Decarli, R., et al. 2017, *ApJ*, 845, 154, doi: [10.3847/1538-4357/aa81cb](https://doi.org/10.3847/1538-4357/aa81cb)
- Villanueva, V., Ibar, E., Hughes, T. M., et al. 2017, *MNRAS*, 470, 3775, doi: [10.1093/mnras/stx1338](https://doi.org/10.1093/mnras/stx1338)
- Vizgan, D., Greve, T. R., Olsen, K. P., et al. 2022, *ApJ*, 929, 92, doi: [10.3847/1538-4357/ac5cba](https://doi.org/10.3847/1538-4357/ac5cba)
- Walter, F., Weiß, A., Downes, D., Decarli, R., & Henkel, C. 2011, *ApJ*, 730, 18, doi: [10.1088/0004-637X/730/1/18](https://doi.org/10.1088/0004-637X/730/1/18)
- Wardlow, J. L., Cooray, A., Osage, W., et al. 2017, *ApJ*, 837, 12, doi: [10.3847/1538-4357/837/1/12](https://doi.org/10.3847/1538-4357/837/1/12)
- Watson, D., Christensen, L., Knudsen, K. K., et al. 2015, *Nature*, 519, 327, doi: [10.1038/nature14164](https://doi.org/10.1038/nature14164)
- Whitaker, K. E., van Dokkum, P. G., Brammer, G., & Franx, M. 2012, *ApJL*, 754, L29, doi: [10.1088/2041-8205/754/2/L29](https://doi.org/10.1088/2041-8205/754/2/L29)
- Wolfire, M. G., Hollenbach, D., & McKee, C. F. 2010, *ApJ*, 716, 1191, doi: [10.1088/0004-637X/716/2/1191](https://doi.org/10.1088/0004-637X/716/2/1191)
- Wolfire, M. G., Vallini, L., & Chevance, M. 2022, *ARA&A*, 60, 247, doi: [10.1146/annurev-astro-052920-010254](https://doi.org/10.1146/annurev-astro-052920-010254)
- Xia, X. Y., Gao, Y., Hao, C. N., et al. 2012, *ApJ*, 750, 92, doi: [10.1088/0004-637X/750/2/92](https://doi.org/10.1088/0004-637X/750/2/92)
- Yamashita, T., Komugi, S., Matsuhara, H., et al. 2017, *ApJ*, 844, 96, doi: [10.3847/1538-4357/aa7af1](https://doi.org/10.3847/1538-4357/aa7af1)
- Young, L. M., Bendo, G. J., & Lucero, D. M. 2009, *AJ*, 137, 3053, doi: [10.1088/0004-6256/137/2/3053](https://doi.org/10.1088/0004-6256/137/2/3053)
- Zanella, A., Daddi, E., Magdis, G., et al. 2018, *MNRAS*, 481, 1976, doi: [10.1093/mnras/sty2394](https://doi.org/10.1093/mnras/sty2394)
- Zhang, Z.-Y., Papadopoulos, P. P., Ivison, R. J., et al. 2016, *Royal Society Open Science*, 3, 160025, doi: [10.1098/rsos.160025](https://doi.org/10.1098/rsos.160025)
- Zhang, Z.-Y., Romano, D., Ivison, R. J., Papadopoulos, P. P., & Matteucci, F. 2018a, *Nature*, 558, 260, doi: [10.1038/s41586-018-0196-x](https://doi.org/10.1038/s41586-018-0196-x)
- Zhang, Z.-Y., Ivison, R. J., George, R. D., et al. 2018b, *MNRAS*, 481, 59, doi: [10.1093/mnras/sty2082](https://doi.org/10.1093/mnras/sty2082)
- Zhao, Y., Yan, L., & Tsai, C.-W. 2016a, *ApJ*, 824, 146, doi: [10.3847/0004-637X/824/2/146](https://doi.org/10.3847/0004-637X/824/2/146)
- Zhao, Y., Lu, N., Xu, C. K., et al. 2016b, *ApJ*, 819, 69, doi: [10.3847/0004-637X/819/1/69](https://doi.org/10.3847/0004-637X/819/1/69)

This figure "orcid-ID.png" is available in "png" format from:

<http://arxiv.org/ps/2410.20684v1>